NASA TECHNICAL NOTE

NASA TN D-7332

NASA TN D-7332

BOUNDARY-LAYER ELECTRON PROFILES FOR ENTRY OF A BLUNT SLENDER BODY AT HIGH ALTITUDE

by John S. Evans, Charles J. Schexnayder, Jr., and Paul W. Huber

Langley Research Center
Hampton, Va. 23665

NATIONAL AERONAUTICS AND SPACE ADMINISTRATION • WASHINGTON, D. C. • JULY 1973

1. Report No.	2. Government Accession No.	3. Recipient's Catalog No.
NASA TN D-7332		

4. Title and Subtitle	5. Report Date
BOUNDARY-LAYER ELECTRON PROFILES FOR ENTRY OF A BLUNT SLENDER BODY AT HIGH ALTITUDE	July 1973
	6. Performing Organization Code
7. Author(s)	8. Performing Organization Report No.
John S. Evans, Charles J. Schexnayder, Jr., and Paul W. Huber	L-8792
	10. Work Unit No.
9. Performing Organization Name and Address	501-04-03-02
NASA Langley Research Center Hampton, Va. 23665	11. Contract or Grant No.
	13. Type of Report and Period Covered
12. Sponsoring Agency Name and Address	Technical Note
National Aeronautics and Space Administration Washington, D.C. 20546	14. Sponsoring Agency Code

15. Supplementary Notes

16. Abstract

New calculations of boundary-layer electron concentration profiles for entry of a blunt-nosed slender body into the earth's atmosphere are compared with previous calculations in which ambipolar diffusion was neglected. The old and new results agree in those flight regimes where ambipolar diffusion is unimportant, but large differences are noted in both peak electron concentration and profile shape at the higher altitudes, where diffusion effects are greatest.

The new results are also compared with flight-measured profiles and with calculated profiles for a viscous-shock-layer theory which was recently reported in the literature. The boundary-layer results and the data agree in most respects. Differences which occur between predicted results and the data in the outer parts of the profile are discussed in terms of the effects of aerodynamic heating of the probes.

17. Key Words (Suggested by Author(s))	18. Distribution Statement
Electron profiles Boundary layer Reentry Radio blackout	Unclassified – Unlimited

19. Security Classif. (of this report)	20. Security Classif. (of this page)	21. No. of Pages	22. Price*
Unclassified	Unclassified	38	$3.00

*For sale by the National Technical Information Service, Springfield, Virginia 22151

BOUNDARY-LAYER ELECTRON PROFILES FOR ENTRY OF A BLUNT SLENDER BODY AT HIGH ALTITUDE

By John S. Evans, Charles J. Schexnayder, Jr.,
and Paul W. Huber
Langley Research Center

SUMMARY

New calculations of boundary-layer electron concentration profiles for entry of a blunt-nosed slender body into the earth's atmosphere are compared with previous calculations in which ambipolar diffusion was neglected. The old and new results agree in those flight regimes where ambipolar diffusion is unimportant, but large differences are noted in both peak electron concentration and profile shape at the higher altitudes, where diffusion effects are greatest.

The new results are also compared with flight-measured profiles and with calculated profiles for a viscous-shock-layer theory which was recently reported in the literature. The boundary-layer results and the data agree in most respects. Differences which occur between predicted results and the data in the outer parts of the profile are discussed in terms of the effects of aerodynamic heating of the probes.

INTRODUCTION

A key factor in the prediction of onset and decay of radio blackout during entry into a planetary atmosphere is the determination of the magnitude and distribution of electron concentration (N_e) in the plasma layer over the entry vehicle. Over the past 10 years considerable progress has been made in understanding and predicting ionized flow fields. In the formula for success, an essential ingredient was the existence of flight-measured data taken over a wide range of entry conditions and related to an analyzable flow field. The RAM (Reentry Attenuation Measurement) project of the Langley Research Center contributed much to both the theoretical and the experimental results. (See ref. 1.)

The importance of nonequilibrium chemistry and of boundary-layer effects was recognized early. (See ref. 2.) Because a complex chemistry system is necessary to calculate trace species concentrations accurately, computation of chemical changes along streamlines in a previously calculated frozen or equilibrium flow field proved to be satisfactory and more economical than a complete flow field calculation with nonequilibrium

chemistry. (See ref. 3.) Except for minor displacement effects, the boundary layer has little influence on N_e profiles for blunt-nosed bodies at the lower altitudes of interest, since the entropy layer is relatively thick and the N_e maxima fall in the inviscid portion.[1] At higher altitudes, where boundary layers are no longer thin relative to the entropy layer and often include the peak of the N_e profile, a method was devised for following streamlines into the boundary layer. (See ref. 3.) By this means it was possible to continue to trace the evolution in time of species concentrations for some distance into the boundary layer. This approach was useful but because ambipolar diffusion of charged particles could not be included, the results are invalid above a threshold altitude. (See ref. 1.)

In this paper the boundary-layer parts of the N_e profiles are calculated by means of a laminar, finite-difference, nonequilibrium, multicomponent diffusion, boundary-layer program (see ref. 4), and the results are compared with previously published profiles obtained by following streamlines into the boundary layer. At the highest altitudes for which measured N_e profiles are available from the RAM studies, boundary-layer theory is not applicable because the mean free path for molecular collisions has become so large that the entire shock layer is viscous. In a recent paper (ref. 5) these experimentally measured profiles were compared with profiles calculated for nonequilibrium fully viscous flow. Since the altitude ranges calculated by means of the two approaches (boundary layer and fully viscous layer) overlap slightly, a comparison with that work is made here also.

SYMBOLS

d_N	nose diameter of body or probe, cm
h	static enthalpy, $cm^2\ sec^{-2}$
l	distance between probe tip and thermocouple, cm
N_e	electron concentration, cm^{-3}
N_i	ion concentration, cm^{-3}
P	specific probe designated by subscripts in figure 10

[1] Electron concentration in the boundary layer may be drastically increased by the presence of easily ionizable substances in the material ablated from the heat protective coating of the entry vehicle.

q_c convective heat flux, W cm^{-2}

R resistance, ohms

T temperature, K

t time, sec

u flow velocity, cm sec^{-1}

w distance between side wall of probes and thermocouple, cm

x distance from nose along body axis, cm

y perpendicular distance from body surface, cm

δ boundary-layer thickness, cm

θ wedge half-angle of probe, deg

λ parameter proportional to heat input to probe, arbitrary units

ρ gas density, g cm^{-3}

ϕ probe sweep angle, deg

Subscripts:

cr critical value

e entry

max maximum

DESCRIPTION OF CALCULATIONS

The RAM C entry body (see fig. 1) was a spherically blunted, 9° half-angle cone with a nose diameter of 30.5 cm. Theoretical treatment of the inviscid flow field for this body, and also of the method for following streamlines into the boundary layer, has been

documented in the literature. (See ref. 3.) Briefly, for given entry speed and altitude, in an atmosphere of known composition, at zero angle of attack, an inviscid flow field around a sphere-cone body was constructed from normalized plots of a large number of inviscid flow field calculations. A laminar[2] boundary-layer program was used to find the thermal properties of the flow field near the surface. The edge conditions were read from profiles of the inviscid properties. Profiles of velocity and density in the boundary layer were then used to determine positions of boundary-layer "streamlines" by mass balance, and nonequilibrium chemical composition was determined along them.

This technique is satisfactory at altitudes low enough to insure that ambipolar diffusion is negligible. In order to be able to calculate N_e profiles at higher altitudes,[3] a finite-difference, laminar, nonequilibrium program for computing boundary-layer properties was acquired from Sandia Laboratories. (See ref. 4.) This program allows for swallowing of inviscid streamlines by specification of the edge conditions. For the RAM C body the vorticity interaction regime, where swallowing is important, lies between 53.4 km and 70.1 km. (See ref. 6.) The wall boundary condition used was equilibrium composition with specified wall temperature.

Some changes were necessary to adapt the program for the present analysis. These were (1) reduction of storage requirement, (2) introduction of variable-step size keyed to the magnitude of changes in chemical composition, (3) replacement of the thermodynamic data,[4] (4) replacement of the means for achieving conservation of elements, and (5) updating the chemical reaction model to include the latest rate constants. The rate constants are given in table I.

DISCUSSION OF RESULTS

In order to identify possible discrepancies between the two methods, concentration profiles were compared for conditions where the effect of ambipolar diffusion was expected to be negligible as well as for those where it was not. Ambipolar diffusion was not important for the altitudes shown in figures 2(a) and 2(b), and the profiles agree well. Edge values of N_e differ in these comparisons because different computed boundary-layer thicknesses lead to different amounts of inviscid streamline swallowing. Also, the inviscid profiles are displaced by different amounts because of different computed values of displacement thickness.

---

[2] Evidence of transition to a turbulent boundary layer at an altitude of about 35 km is cited in reference 1.

[3] And, also, to develop a capability to account for ionization in the boundary layer caused by the presence of alkali metals in material ablated from the body surface.

[4] The thermodynamic data replacement was to insure that thermodynamic properties would be identical when the data are compared with previous work.

The profiles of figure 2(c) were computed for an altitude of 71.0 km, which is the upper limit cited in reference 1 for neglect of ambipolar diffusion of the charged species. Based on the present results, the upper limit for neglect of ambipolar diffusion is between 60 and 70 km.

Another indication of the onset of diffusion effects as the altitude increases is the plots in figure 3 of calculated peak N_e against altitude.[5] The dashed lines show the values calculated by means of the older technique of following streamlines into the boundary layer. The solid lines are the later results. The rapid decrease in measured peak N_e at high altitude seems to match the new curves better than the old ones.

Figure 4 shows a comparison between electron concentration profiles measured on the RAM C-III flight and the corresponding profiles calculated by use of the boundary-layer theory described. Lines representing upper limits for the magnitudes of the N_e profile peaks as determined by the S-band diagnostic antenna (ref. 7) are also shown. One of these lines is the peak value of N_e as measured at $x/d_N = 2.3$, the location of the diagnostic antenna. The other is the same peak value divided by 2 to adjust it to the $x/d_N = 4$ body station. (A factor of 2 reduction between these two stations is predicted by the boundary-layer theory results.) The agreement in figure 4(a) between boundary-layer theory and the experimental data points is good from the body surface out to a distance of about 9 cm; beyond 10 cm the data points rise rather than fall as theory predicts. The ionization currents collected by the outer probes at this altitude and lower altitudes are believed to be masked by leakage currents in the insulators, which are increasingly degraded by aerodynamic heating as the altitude decreases.

Leakage of the probe insulators due to heating was recognized and discussed in a previous publication. (See ref. 8.) The leakage effects occur first at the outermost probe and affect probes closer to the body surface as altitude decreases. A previously published criterion for discarding probe data for some of the outermost probes was based on temperatures measured in flight by thermocouples beneath the insulator surface. (See ref. 8.) A later investigation based on surface heating effects is described in the appendix. This later study indicates that the heating effects may have had an earlier onset and may have involved more probe positions than was previously believed to be the case. The fixed-bias probe positions believed to be affected are indicated in figure 4 by the solid symbols. Note, however, that the symbols for swept-bias probe data in figure 4(b) at $y = 6.5$ cm and $y = 9.5$ cm are not solid, even though the fixed-bias data in this region are believed to be suspect according to the criterion set forth in the appendix. The point at $y = 6.5$ cm can be considered to be a borderline case, but the point at $y = 9.5$ cm is well within the heating region for the fixed-bias probes.

[5] All data in figures 3(a) and 3(b) are from RAM C-II, which had no alkali metal contamination in the flow. The data in figure 3(c) are from RAM C-III, for which alkali contamination effects were present but were negligible above 65 km.

An analysis of RAM C-III data was performed by W. L. Jones of the Langley Flight Instrumentation Division to determine the sensitivity of the swept-bias probe interpretation to resistive leakage currents. The results showed that the occurrence of significant probe leakage was easy to distinguish because of the resulting distortion of the nonlinear (diode-like) Langmuir probe current-voltage characteristic. Furthermore, since the ion current "saturates" for negative bias larger than a few volts, the linear leakage current produces a greater error at the -5 volt (fixed-bias probe) potential. The conclusions of his analysis were (1) the error in N_e inferred from a swept-bias probe is about a factor of 3 smaller than that for a fixed-bias probe, (2) maximum error in the N_e inferred from a swept-bias probe before heating becomes apparent could be as large as a factor of 4 increase over the correct value, and (3) leakage is significant (error exceeds a factor of 4) at the 9.5-cm swept-bias probe below 65.0-km altitude. These conclusions are consistent with figure 5 which shows the altitude plots of N_e for both swept- and fixed-bias probes and the profile peak N_e measured in the S-band diagnostic antenna experiment. (See ref. 7.) The data from the outermost probe (fig. 5(d)) show a large increase of N_e with decreasing altitude during the no-injection period near an altitude of 65 km. The fact that such a large increase is not seen for the other three probes along with the observation that N_e greatly exceeds the profile peak values measured with the S-band diagnostic antenna[6] strongly suggests the onset of heating. Because of this observation, a factor of 4 error bar is placed on the value of N_e plotted at 9.5 cm in figure 4(b).

Additional support for the hypothesis that fixed-bias probe heating is significant at altitudes of 70 km and lower is present in the RAM C-III thermocouple records and the RAM C-II and RAM C-III fixed-bias probe data. The RAM C-II probe data (see fig. 3) continue to rise steeply at altitudes lower than 70 km, whereas the slower rise of the RAM C-III data in the same region is attributed to cooling of the RAM C-III probes by the liquid injected into the flow. (RAM C-II had no injection experiment.) To avoid confusion between data collected under very different heating conditions, only RAM C-III data were used for analysis of heating effects. The C-II data can be obtained from reference 8, 9, or 10.

The agreement of the boundary-layer theory with the data in figure 4 is good when one considers that because of probe heating effects, the values of N_e shown by the solid symbols are higher than the correct values and that the difference increases with distance from the body surface. The measured profiles are perhaps a few centimeters thicker than the theory predicts, but when the approximations in the theory are considered, this difference is not significant. Viscous-layer profiles from reference 5 are compared with

[6] The S-band profile peaks were measured at $x/d_N = 2.3$. Since the plasma was expanding and recombining, it is reasonable to believe that the N_e peaks were even lower at $x/d_N = 4.0$. (The boundary-layer theory predicts a factor of 2 lower.)

Langmuir probe data in figures 6 and 7. (Fig. 6 is from ref. 9.) Note that the fixed-bias probe results in figure 7 are the same as those presented in reference 5 but that in order to show trends in profile shape, the data have been presented in the form of points with error bars[7] rather than as wide shaded bands. Also, swept-bias probe results presented herein are the result of an improved analysis by one of the authors (W. L. Jones) of reference 5.

At 83.8 and 80.8 km, the viscous shock layer curves from reference 5 agree well with the data except near the shock, where the data do not support an upswing. At 76.2 km, the data have the form of a wide, flat peak with definite indication of a fall-off of N_e in the outer portion. Again, there is no support for an upswing. Some indication of an apparent upswing is visible at 71.0 km, but the points responsible have already been questioned as being too high because of probe heating. The criteria used to decide when heating may be important are discussed in the appendix, where it is also demonstrated by sample calculations that an upswing of the outer part of a profile is precisely what one would expect in the initial heating phase.

The 71.0-km probe data of figure 7 also appear in figure 4(a), where they are compared with the profile calculated from boundary-layer theory. (Recall that the boundary-layer theory profile probably should be a few centimeters thicker.) Three additional fixed-bias probe points measured at 70.1 km are shown in this figure because they offer support for the idea that the outer probes are affected by heating. (The other points on the profile at 70.1 km were omitted because they were practically identical with those for 71.0 km.)

The "instantaneous"[8] experimental profiles in figure 6 (taken directly from ref. 9) are better suited to illustrate the peaked shapes of the N_e profiles than are the time-averaged data (subject to body-motion uncertainty) in figure 7. These data are read at a given instant in time so that, relative to each other, each point is subject only to instrument error, which is on the order of ±20 percent. Therefore, the shape of the profile is well determined even though there is a bias of larger uncertainty (up to a factor of 2) when identifying the profiles with a given angle of attack. Because of a lack of high-altitude acceleration data, the angles of attack are not known for the curves in figure 6. (The angle of attack probably did not exceed 5°. See ref. 11.) According to reference 12, angle of attack does not alter the general shape of the profile, but changes only the peak value of N_e and the profile thickness.

Further support for believing that the distribution of electrons in the shock layer is more like that predicted by the boundary-layer theory than that predicted by the

---

[7] In laboratory calibrations the probe readings were good to ±20 percent. The error bars represent local extremes of fluctuations caused by body motions – principally angle of attack. The data points in figure 7 are time averages during the no-injection periods.

[8] Each profile was obtained in approximately 27 msec.

viscous-layer theory of reference 5 is obtained by examining the theoretical and experimental (ref. 7) S-band attenuation results in figure 8. The electromagnetic wave attenuation was calculated for the S-band antenna by using a near-field analysis (ref. 13) and the N_e profiles from both the viscous-layer and the boundary-layer theories. Both range and pattern effects have been taken out of the experimental data, so that it presumably represents only attenuation caused by the plasma. Although both calculated attenuation results are high relative to that observed, the curve based on the viscous-layer profiles is much higher than the one based on the boundary-layer profiles. The boundary-layer theory would predict the start of attenuation at an altitude closer to the experimentally observed beginning of attenuation than the viscous-layer theory would. A parametric study by C. T. Swift of the Langley Flight Instrumentation Division established the sensitivity of the S-band attenuation to scaling[9] the N_e profiles. His results showed that the observed attenuation would be predicted by the boundary-layer N_e profiles if their peaks were decreased in magnitude by a factor of about 2; whereas for the viscous-layer theory, the peak N_e (at the edge of the shock) had to be reduced by a factor of $3\frac{1}{2}$ to 4 to match the observed attenuation.

Measured S-band antenna admittance is compared with calculated admittances (refs. 13 and 14) for both theoretical profiles in figure 9. The boundary-layer profiles give values closer to experiment, but neither set of profiles is completely consistent with the simultaneous admittance and attenuation measurements for RAM C-III even when both are scaled.

Another question can be raised about the viscous-layer theory results from reference 5. Although reasonably good correlation with the flight data at the rear of the vehicle was obtained, the theory overpredicted N_e values measured by microwave reflectometers on RAM C-II at the more forward body stations $\left(x/d_N = 0.15 \text{ and } x/d_N = 0.76\right)$ by factors as large as 20. Over the altitude range (71 km and lower) appropriate for the boundary-layer theory, agreement of results from boundary-layer theory with results from reflectometer measurements is obtained at all body stations, as can be seen in figures 3(a) and 3(b).

CONCLUDING REMARKS

A comprehensive theoretical method was employed to confirm previous studies that indicated the need to include ambipolar diffusion in boundary-layer calculations of N_e profiles for RAM-C vehicles above an altitude of about 65 km. For these flights the comparison of theory and flight data indicates that the transition from fully viscous-shock-layer flow to boundary-layer flow takes place at no lower than 70-km altitude. Based on

[9] Profile shapes were preserved as the peak N_e was varied over a range which included values above and below $(N_e)_{cr}$.

calculated surface heating variation for the Langmuir probes, results indicate that some of the probe insulators may have been affected by heating in such a way as to change the character of the measured N_e profiles at the lower altitudes. Satisfactory agreement between measured and boundary-layer calculated N_e profiles is obtained when the probe results that are considered to be questionable by the criteria developed here are deleted.

Langley Research Center,
National Aeronautics and Space Administration,
Hampton, Va., June 18, 1973.

APPENDIX

ELECTRICAL LEAKAGE IN THE LANGMUIR PROBES

All three of the RAM C flights used Langmuir probe rakes which measured the ion saturation current[10] flowing from the plasma into the probes for a fixed negative bias of 5 volts. Each probe was in series with a 400-ohm load resistor and all the probes of a given rake were simultaneously biased, the reference electrode serving as the common positive electrode. The physical and electrical characteristics of the probes, as well as the tests made to establish these characteristics, are described in detail in reference 9. Less detailed descriptions are found in references 8 and 10.

There are two types of electrical leakage which can alter the current flowing through the load resistors and hence lead to false indication of the actual plasma current flow. First, leakage can occur along the surface of the BeO dielectric material at the leading edge of the probe rake between adjacent probes if the heating of the leading edge is sufficient to lower its surface resistance significantly. Second, leakage current can flow along the BeO surface between any probe and the reference electrode. This type might not occur quite as early in the entry as the probe-probe leakage, since the surface of the rake wedge is inclined at a more oblique angle to the flow than the leading edge is. On the other hand, the probe circuitry is much more sensitive to the latter type leakage than to the probe-probe type, as can be seen from figure 10 where the effects caused by both types of leakage are illustrated for a fixed-bias Langmuir probe circuit with four simultaneously biased probes. The curve drawn through the circles represents the outer part of an assumed profile where there is no leakage occurring. This shape is similar to the outer part of the theoretical profiles. The equivalent plasma resistances for the assumed profile are taken from reference 9 and are shown in the circuit diagram in the figure. For the case of probe-probe leakage amounting to a dead short between the outer two probes (curve drawn through the squares) it is seen that the outer profile is raised slightly but is still much lower than the peak N_i value of 10^{11} cm^{-3}. The other two curves are for cases where probe-reference electrode leakage is occurring through a 25-kΩ leakage path. One of these cases includes some probe-probe leakage as well (diamonds, R_1 = 1000 ohms), but the upswing in the outer profile is due to the probe-reference electrode leakage in both cases. Since heating of the probes will be shown to increase with distance from the body surface, this upswing trend would be expected to continue if more probes were included in the analysis. In summary, figure 10 shows that surface leakage effects can account for changes in apparent N_i profile shape from a steep fall-off in the outer part to an upswing above the inner peak. The curve represented by the diamonds (with both types of leakage)

---

[10] Under the assumption that $N_i = N_e$ in the plasma, measurement of N_i is equivalent to measurement of N_e.

is probably the most reasonable one since the leading-edge BeO surface should be hotter than the wedge surface, and the path length between probes is shorter than the path from probe to reference electrode and, as a result, $R_1 < R_2$. (The values of leakage resistance used in this simulation are not necessarily representative of those which occurred during the flight.)

In view of this discussion, let us now consider the RAM-C Langmuir probe data as compared with expected trends established by theoretically predicted profiles. Below an altitude of 71 km, the boundary layer is not expected to fill the shock layer, even at the nose of the vehicle, according to the nonequilibrium boundary-layer vorticity interaction theory used herein. Conceptual arguments further imply that the boundary layer will not fill the shock layer at the Langmuir probe station at altitudes even higher than 71 km because of boundary-layer breakaway. The theory also predicts that a peaked N_i profile is to be expected at this station, and that the peak moves toward the surface and increases in magnitude as the altitude decreases from the 71 km, or higher, initial case. By looking at figures 4, 6, and 7, one can see that this trend is indeed observed on RAM C-III until the altitude decreases to 70.1 km, where the outer portion of the ion profile begins rising to values greater than the inner peak. At still lower altitudes (65.2 and 61.6 km), the peak continues to move in and to rise, but the N_i values measured in the outer portion also move in and rise still more.

This qualitative result suggests that heating effects, most likely probe-reference electrode leakage, are beginning to affect the currents collected at the outer probes at about 71 km, and that they increase in magnitude and move closer to the surface as the altitude decreases. Estimates of probe heating qualitatively verify this behavior, although quantitative estimates are uncertain because of the large degree of chemical nonequilibrium, the transitional nature of the fluid dynamical regime, and the uncertainty of BeO surface catalycity for these conditions.

If one assumes that continuum fluid dynamics governs the flow near the probe rake, then the convective heat flux at the tip of the rake varies as (ref. 15)

$$q_c \propto \left(\rho/d_N\right)^{1/2}\left(2uh + u^3\right) \tag{A1}$$

where $h = \Sigma\, a_i h_i$, a_i is the mass fraction, and h_i is the heat content of species i due to thermal motions. The $2uh$ term allows for the high enthalpy, relatively low Mach number, nature of the shock layer flow, and for the assumption that the energy in dissociation will not be available to heat the probe because of the short compression time at the tip. This relation can be applied to the swept cylinder case herein, since only the relative change in heating along the rake is being considered.

The continuum-flow assumption is more appropriate for the altitude range where heating is critical, since the rake tip diameter is greater than the neutral-neutral mean free path in the plasma ahead of the outer RAM C-III probes at 71.0 km and is greater for all the probes at 65.2 km and lower. If free molecular flow were assumed, the only difference would be that density would appear to the first power rather than to the one-half power.

By using the nonequilibrium flow field results described herein, expression (A1) was evaluated at all the Langmuir probe positions over a range of altitudes from 71.0 km to 61.0 km; viscous shock layer values (ref. 5) were used for the higher altitudes. By integrating the results at each Langmuir probe station over the reentry time to given altitudes, the quantity

$$\lambda = \int_{t_e}^{t} \rho^{1/2}\left(2uh + u^3\right)dt \tag{A2}$$

was obtained; this quantity is proportional to the total leading-edge heat input. The variation of λ with altitude and probe position is shown in figure 11, which illustrates relative heating effects on the different probes of the RAM C rakes as a function of altitude. If it is assumed that the effects of leakage due to heating are first manifested at an altitude of 70.1 km and at about $y = 9$ or 10 cm (see figs. 4 and 7), then one can predict which probes will be affected by heating at other altitudes by using the same value of λ in figure 11. A critical value of λ can also be assigned for the RAM C-I and C-II flights by using the relation

$$\lambda = \lambda_{C\text{-III}} \frac{\cos \phi_{C\text{-III}}}{\cos \phi_{C\text{-I,II}}} \frac{\left(d_N\right)_{C\text{-I,II}}}{\left(d_N\right)_{C\text{-III}}} \tag{A3}$$

which accounts for the difference in tip diameter and sweep angle of the rakes. This value of λ is 15 percent higher (that is, lower heat load) than the value for RAM C-III, and it is also shown[11] in figure 11. The pertinent data (ref. 9) for the different RAM C rakes are given in table II and figures 1 and 12. The thermocouple rakes and Langmuir probe rakes were physically identical in a given flight except that thermocouples were embedded in the BeO insulator in contrast to the probe electrodes which protruded through the leading edge. The filled symbols in figures 4 and 7 represent those fixed-bias data for which λ is higher than the critical value in figure 11.

[11] In the context of probe heating relative to that for RAM C-III this value of λ would only apply to RAM C-I. The value of λ for RAM C-II is probably lower (higher heat load), since there was no material injection to cool the probe as there was on RAM C-I and C-III. (See fig. 3 and discussion in text.)

Although this approach is useful in estimating the probe heating variation with altitude and distance from the vehicle surface, a more direct approach would be an experimental correlation of measured leakage resistance with thermocouple readings under simulated reentry conditions. Some tests of this nature were made (ref. 9), but because of test constraints and later changes in thermocouple and rake geometry, quantitative application to the RAM C flights cannot be made. For example, the stagnation temperature of the tunnel was below the melting temperature of the BeO, although reentry stagnation temperatures are much higher than the melt temperature $(T_{melt} = 2600\ K)$. Also, the tests were limited to a duration of less than 3 seconds, even though the thermocouple temperature was still rising significantly at the test termination $(T_{max} \approx 950\ K)$. Most important, however, is the fact that the measured thermocouple temperatures must always be much smaller than the leading-edge surface temperatures, and, unfortunately, this difference is greatest for the RAM C-III rake where, because of the rake's longer extension and lower sweep angle, the heating effects are largest. The problem in all three cases is that the embedded thermocouple is closer to the wedge surface than it is to the leading edge. (See fig. 12 and table II.) Also, for C-III the thermocouple is considerably farther from the leading edge and the wedge angle is much smaller than it is for the RAM C-I. (The wedge surfaces are, of course, much cooler than the leading edge.) Both of these factors significantly increase ΔT between the thermocouple and the leading edge for C-III as compared with C-I (which the tunnel test configuration most closely resembles). This difference appears to be experimentally confirmed by the flight data (ref. 9), where the measured C-III thermocouple temperatures are much lower than those of C-I for given altitude and distance from the vehicle surface, in spite of the fact that the leading-edge heating for C-III is about 15 percent higher.

This discussion leads us to conclude that Langmuir probe current leakage due to heating could have affected some of the RAM C measured ion profiles. Leakage between probes and the reference electrode appears to be the most serious type, even though probe-probe leakage resistance values are lower. A consistent and meaningful correlation of the flight data with theoretical flow field concepts is obtained by restricting comparison to probes for which λ is within the critical boundaries shown in figure 11. It is also suggested that the critical thermocouple temperature criterion of 1366 K used by Jones (ref. 9) in interpreting the RAM C data was too high. On the basis of the criterion illustrated in figure 11, the critical thermocouple temperature is between 533 K and 811 K for RAM C-III and around 811 K for RAM C-I.

REFERENCES

1. Huber, P. W.; Evans, J. S.; and Schexnayder, C. J., Jr.: Comparison of Theoretical and Flight-Measured Ionization in a Blunt Body Re-Entry Flowfield. AIAA J., vol. 9, no. 6, June 1971, pp. 1154-1162.

2. Evans, John S.; and Huber, Paul W.: Calculated Radio Attenuation Due to Plasma Sheath on Hypersonic Blunt-Nosed Cone. NASA TN D-2043, 1963.

3. Evans, John S.; Schexnayder, Charles J.; and Huber, Paul W.: Computation of Ionization in Re-Entry Flowfields. AIAA J., vol. 8, no. 6, June 1970, pp. 1082-1089.

4. Blottner, F. G.: Prediction of Electron Density in the Boundary Layer on Entry Vehicles With Ablation. The Entry Plasma Sheath and Its Effects on Space Vehicle Electromagnetic Systems, Vol. I, NASA SP-252, 1971, pp. 219-240.

5. Kang, Sang-Wook; Jones, W. Linwood; and Dunn, Michael G.: Theoretical and Measured Electron-Density Distributions at High Altitudes. AIAA J., vol. 11, no. 2, Feb. 1973, pp. 141-149.

6. Blottner, F. G.: Viscous Shock Layer at the Stagnation Point With Nonequilibrium Air Chemistry. AIAA J., vol. 7, no. 12, Dec. 1969, pp. 2281-2288.

7. Schroeder, Lyle C.; Swift, Calvin T.; Akey, Norman D.; and Beck, Fred B.: Material Injection Alleviation and Plasma Diagnostic Measurements During the RAM C-III Flight. AIAA Paper No. 72-690, June 1972.

8. Jones, W. Linwood, Jr.; and Cross, Aubrey E. (With appendix B by Lorraine F. Satchell and appendix C by William L. Weaver): Electrostatic-Probe Measurements of Plasma Parameters for Two Reentry Flight Experiments at 25 000 Feet Per Second. NASA TN D-6617, 1972.

9. Jones, William Linwood, Jr.: Probe Measurements of Electron Density Profiles During a Blunt-Body Reentry. Ph. D. Thesis, Virginia Polytech. Inst. and State Univ., June 1971.

10. Jones, W. Linwood, Jr.; and Cross, Aubrey E.: Electrostatic Probe Measurements of Plasma Surrounding Three 25 000 Foot Per Second Reentry Flight Experiments. The Entry Plasma Sheath and Its Effects on Space Vehicle Electromagnetic Systems, Vol. I, NASA SP-252, 1971, pp. 109-136.

11. Weaver, William L.; and Bowen, John T.: Entry Trajectory, Entry Environment, and Analysis of Spacecraft Motion for the RAM C-III Flight Experiment. NASA TM X-2562, 1972.

12. Schexnayder, Charles J., Jr.; Huber, Paul W.; and Evans, John S.: Calculation of Electron Concentration for a Blunt Body at Orbital Speeds and Comparison With Experimental Data. NASA TN D-6294, 1971.

13. Bailey, Marion C.; and Swift, Calvin T.: Input Admittance of a Circular Waveguide Aperture Covered by a Dielectric Slab. IEEE Trans. Antennas & Propagation, vol. AP-16, no. 4, July 1968, pp. 386-391.

14. Dunn, Michael G.; Blum, Richard J.; Swift, Calvin T.; Beck, Fred B.; and Grantham, William L.: Antenna Admittance Determination of Electron Density. AIAA J., vol. 11, no. 7, July 1973, pp. 1018-1024.

15. Bobbitt, Percy J.: Problems of Atmospheric Entry. Performance and Dynamics of Aerospace Vehicles, NASA SP-258, 1971, pp. 175-288.

TABLE I.- REACTIONS AND RATES USED FOR CALCULATIONS

Reaction	Forward-rate constant,* k_f			Reverse-rate constant,* k_r			Third body M
	A	B	C	A	B	C	
$O_2 + M \rightleftharpoons O + O + M$	3.6×10^{18}	-1.0	59 400	3.0×10^{15}	-0.5	0	N, NO
$O_2 + O_2 \rightleftharpoons O + O + O_2$	3.3×10^{19}	-1.0	59 400	2.7×10^{16}	-.5	0	
$O_2 + N_2 \rightleftharpoons O + O + N_2$	7.2×10^{18}	-1.0	59 400	6.0×10^{15}	-.5	0	
$O_2 + O \rightleftharpoons O + O + O$	9.0×10^{19}	-1.0	59 400	7.5×10^{16}	-.5	0	
$N_2 + M \rightleftharpoons N + N + M$	1.9×10^{17}	-.5	113 100	1.1×10^{16}	-.5	0	O_2, O, NO
$N_2 + N \rightleftharpoons N + N + N$	2.1×10^{22}	-1.5	113 100	1.2×10^{21}	-1.5	0	
$N_2 + N_2 \rightleftharpoons N + N + N_2$	4.8×10^{17}	-.5	113 100	2.7×10^{16}	-.5	0	
$NO + M \rightleftharpoons N + O + M$	4.0×10^{20}	-1.5	75 600	1.0×10^{20}	-1.5	0	O_2, N_2
$NO + M \rightleftharpoons N + O + M$	7.9×10^{21}	-1.5	75 600	2.0×10^{21}	-1.5	0	O, N, NO
$NO + O \rightleftharpoons O_2 + N$	3.2×10^{9}	1.0	19 700	9.6×10^{11}	.5	3600	
$N_2 + O \rightleftharpoons NO + N$	6.8×10^{13}	0	37 500	1.5×10^{13}	0	0	
$N + O \rightleftharpoons NO^+ + e^-$	2.4×10^{10}	.5	32 400	4.0×10^{20}	-1.2	0	

*Form of rate constant is $k = AT^B \exp(-C/T)$ with k in $cm^3/mole\ sec$ or $cm^6/mole^2\ sec$.

TABLE II.- PERTINENT DIMENSIONS OF RAM C RAKES

	RAM C-I	RAM C-II	RAM C-III
Rake sweepback angle, ϕ, deg	45	45	30
Wedge half-angle, θ, deg	30	30	15
BeO leading-edge diameter, d_N, cm	0.088	0.088	0.099
Thermocouple, embedded depth			
From leading edge, l, cm	0.051	0.081	0.094
From wedge surface, w, cm	0.046	0.061	0.058

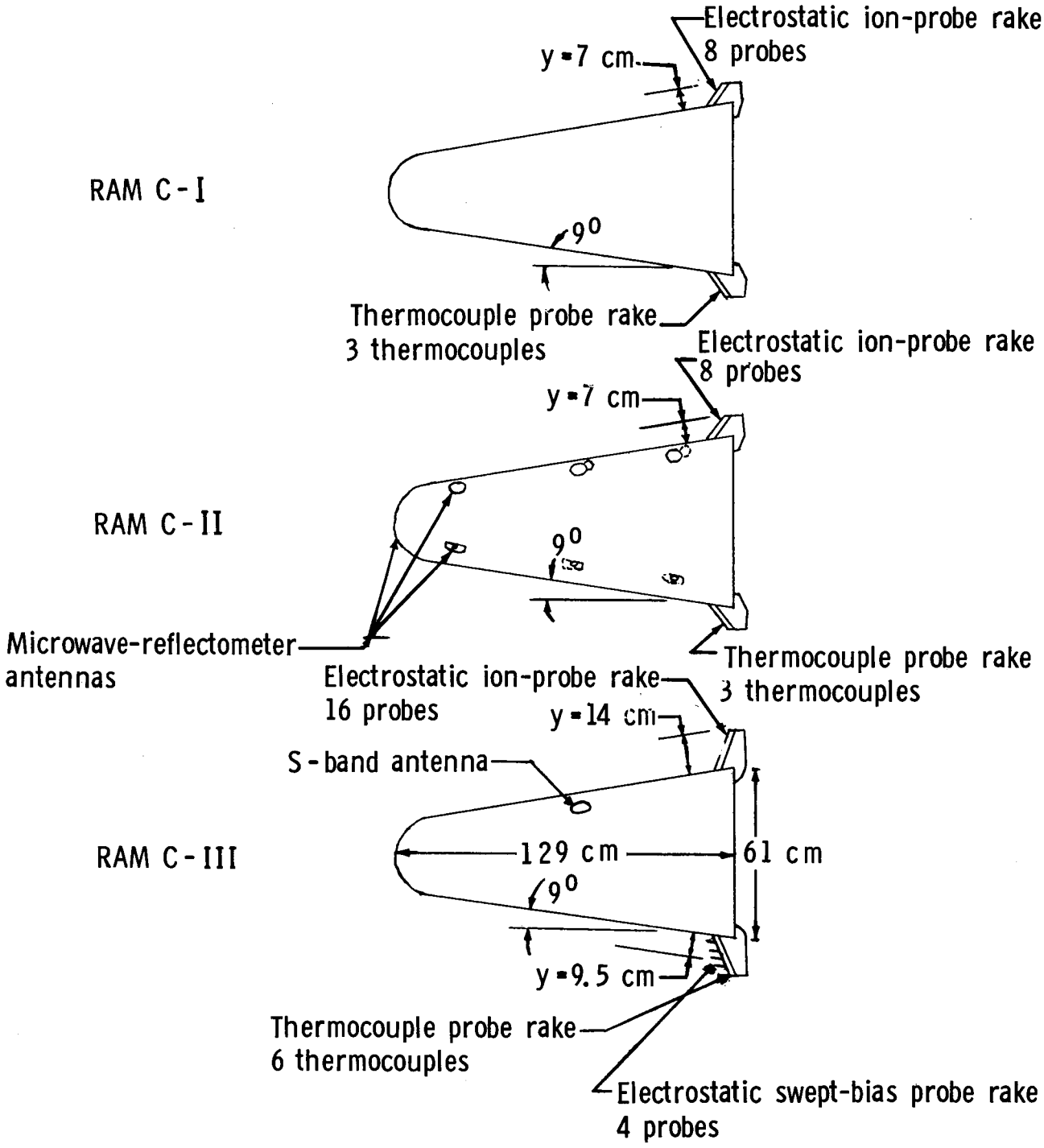

Figure 1.- RAM C-I, C-II, and C-III configurations.

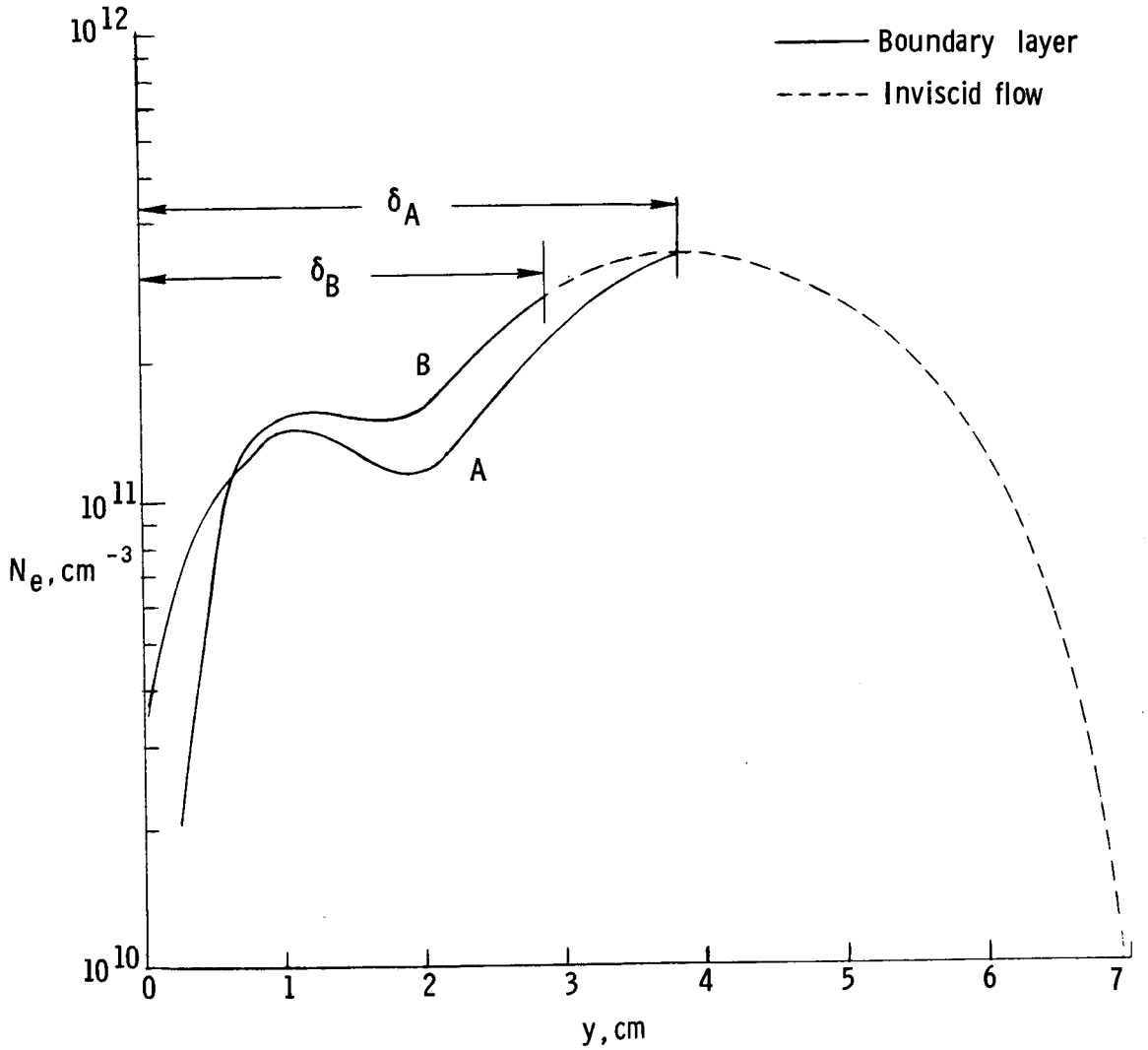

(a) 53.4 km.

Figure 2.- Comparison of computed N_e profiles at $x/d_N = 4$ from nonequilibrium, multicomponent diffusion program (curve A) with those from the streamline method (curve B).

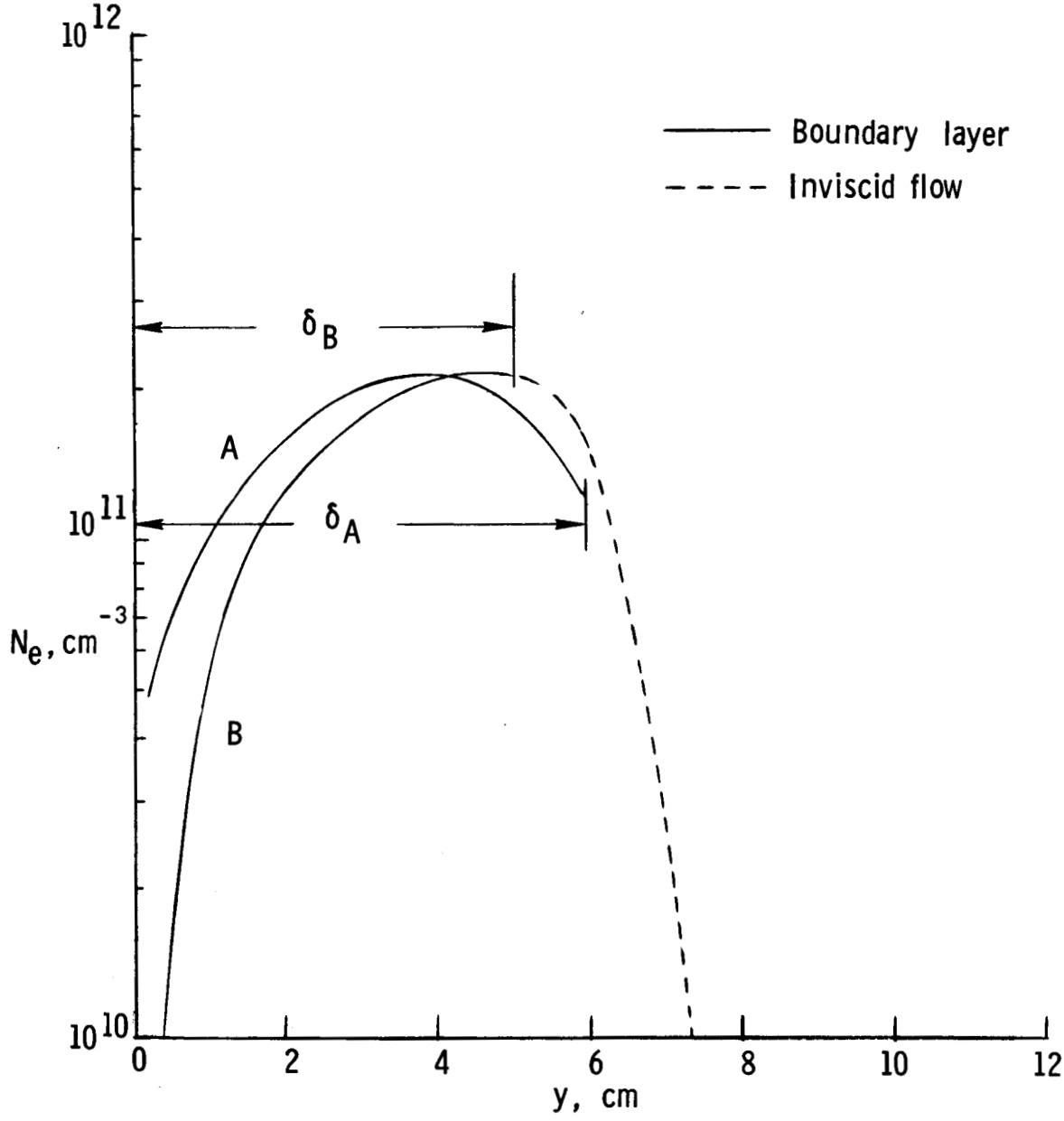

(b) 61.6 km.

Figure 2.- Continued.

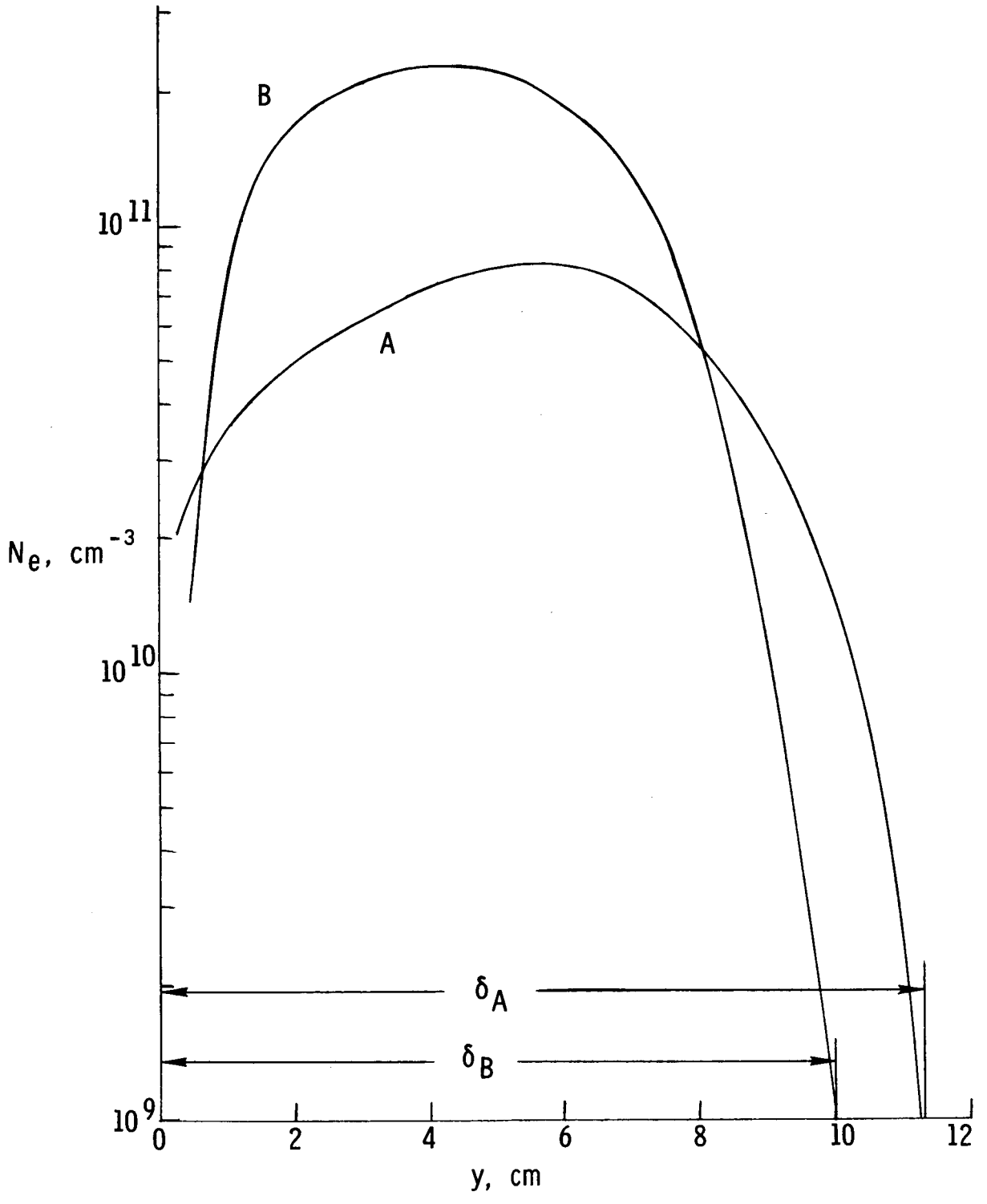

(c) 71.0 km.

Figure 2.- Concluded.

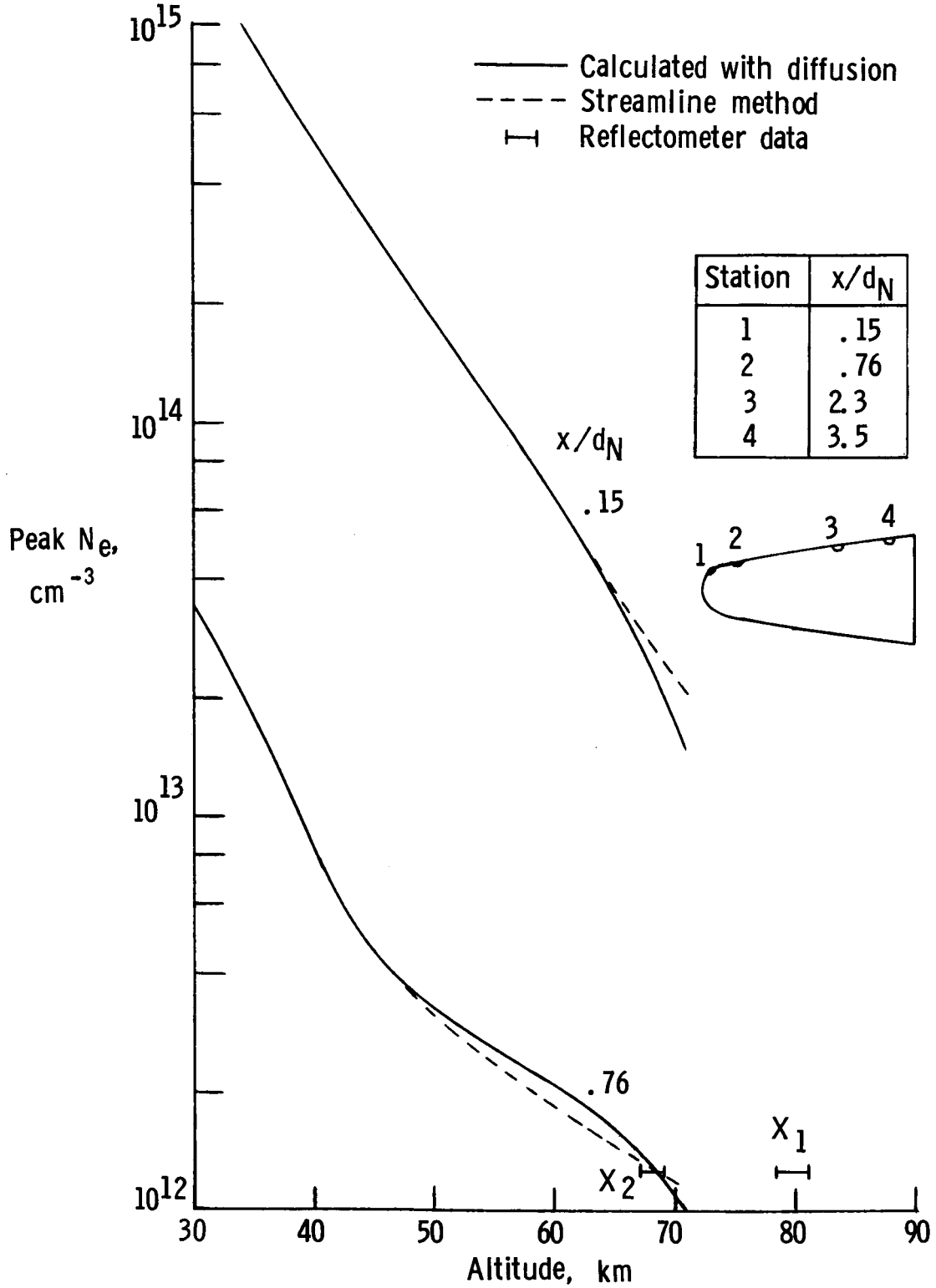

(a) Compared with experimental values in nose region of RAM C-II. (Subscripts on X-band reflectometers refer to station numbers.)

Figure 3.- Variation of peak N_e with altitude.

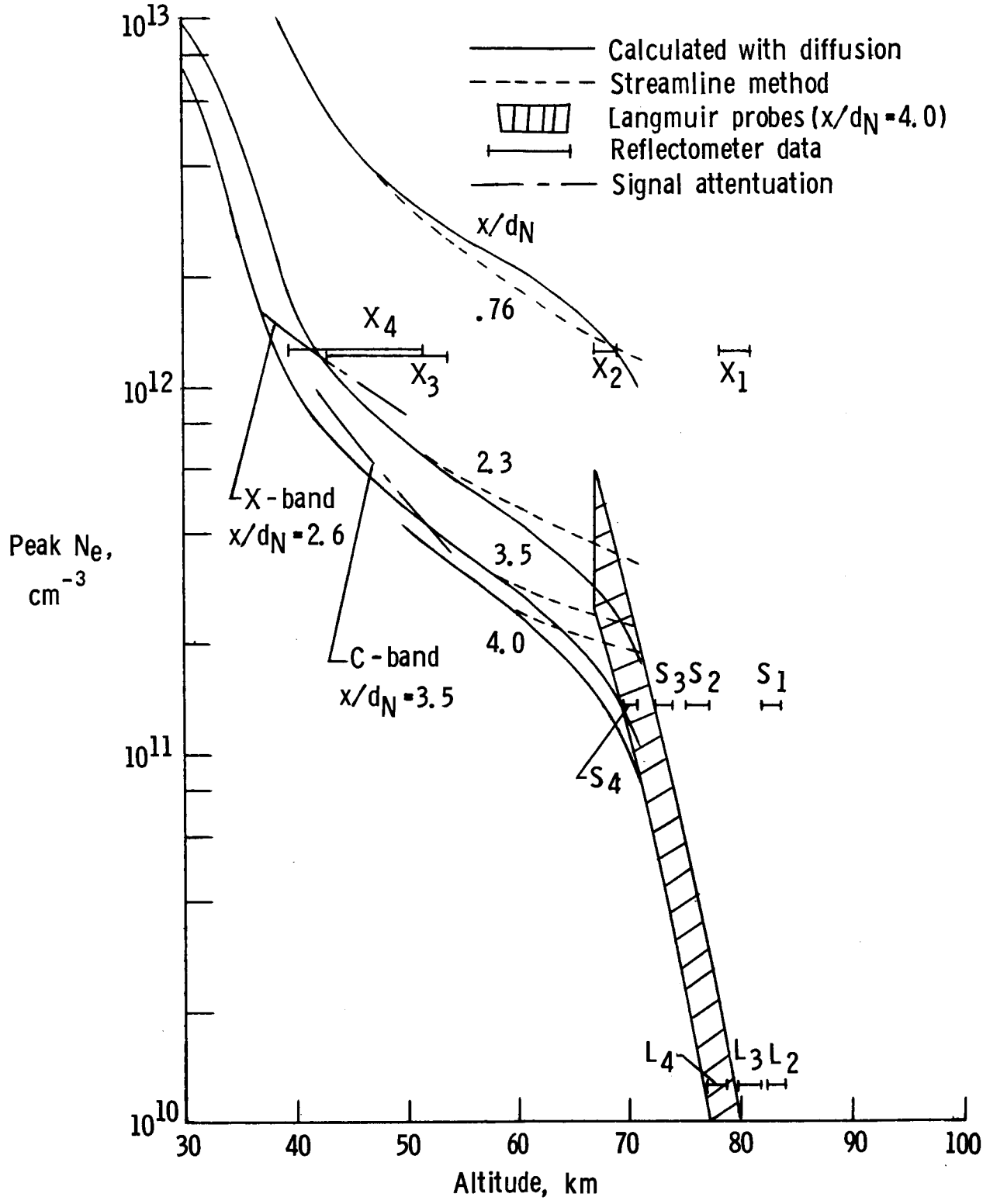

(b) Compared with experimental values on afterbody of RAM C-II. (Subscripts on X-, S-, and L-band reflectometers refer to station numbers.)

Figure 3.- Continued.

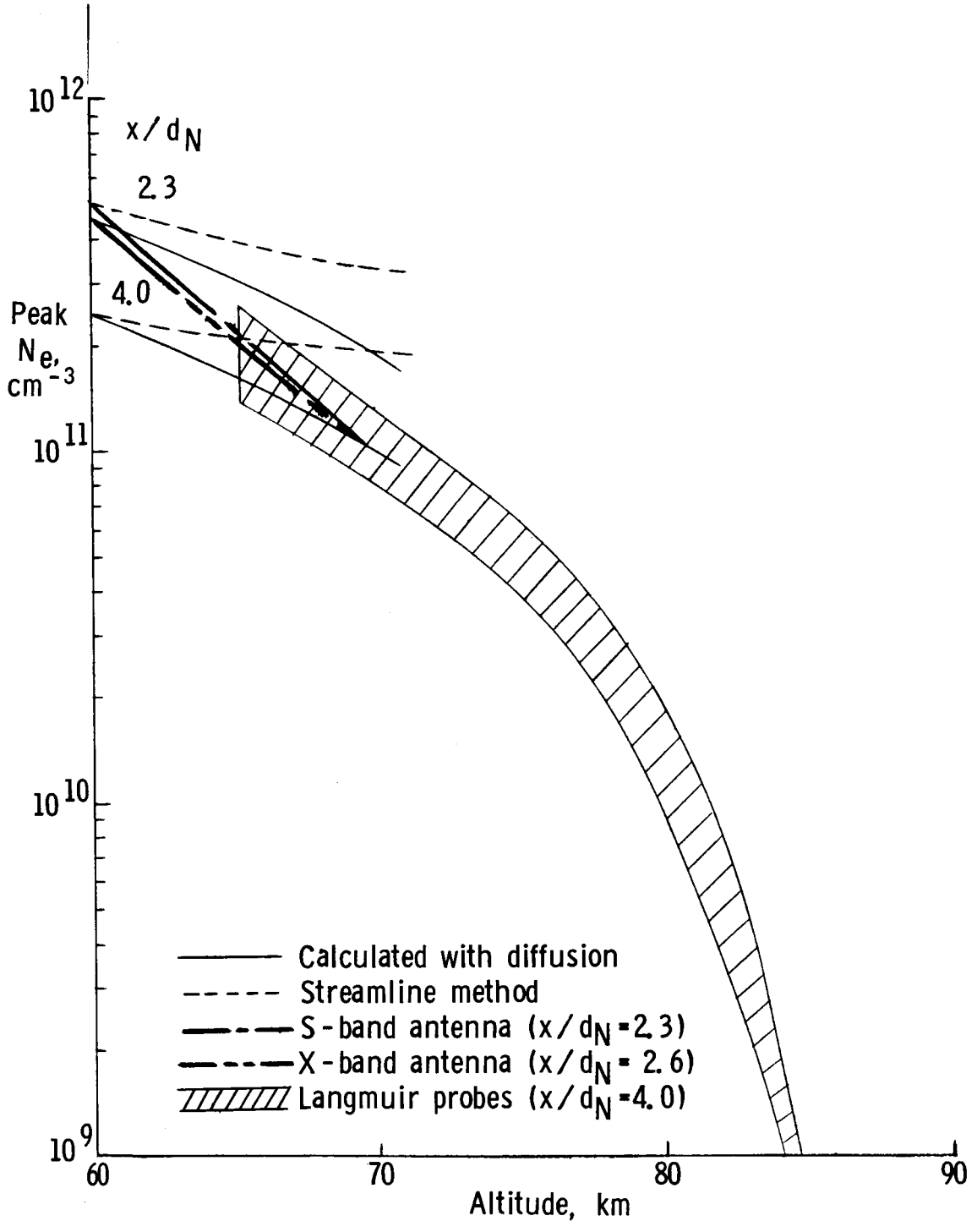

(c) Compared with experimental values on afterbody of RAM C-III.

Figure 3.- Concluded.

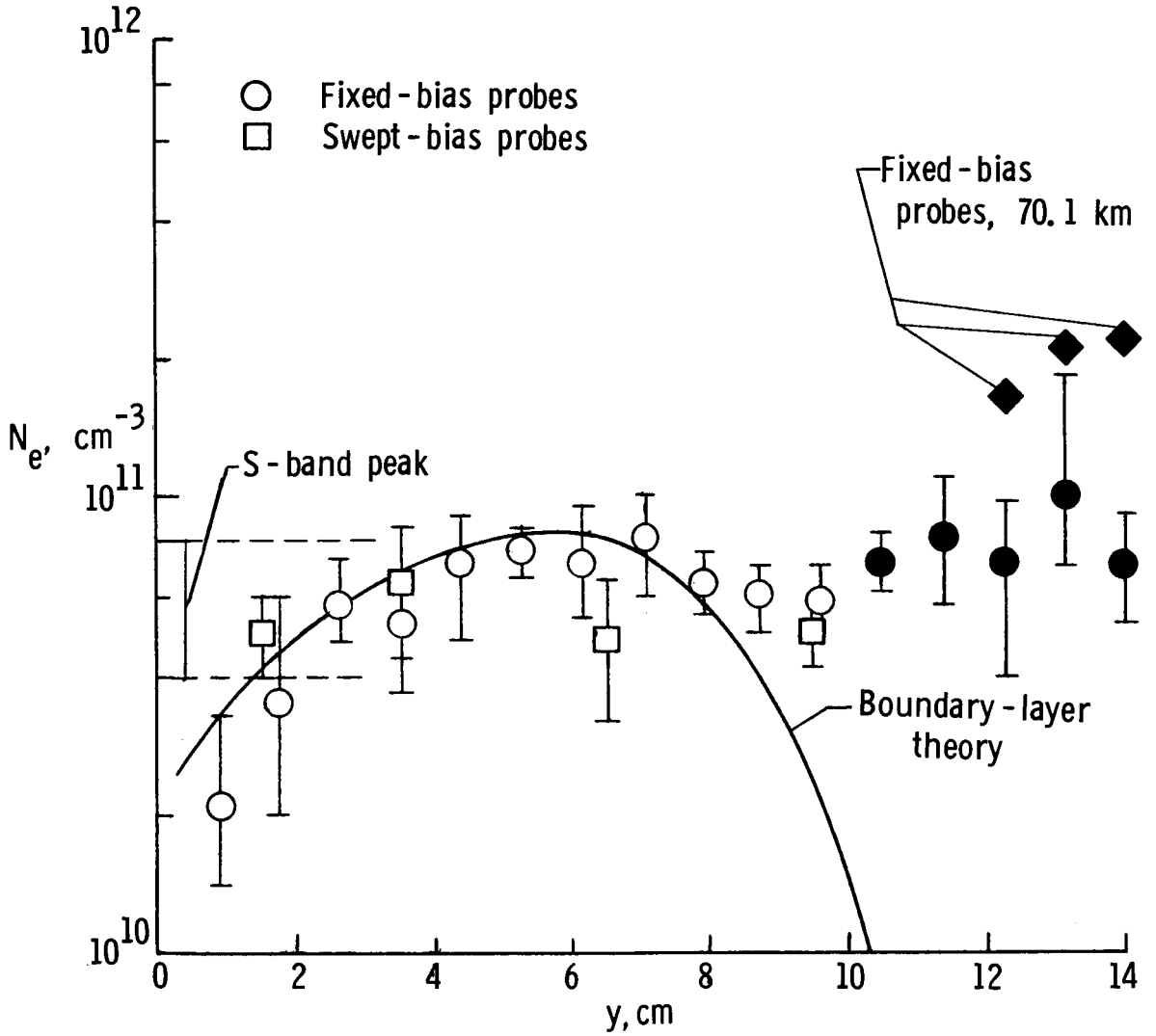

(a) 71.0 km.

Figure 4.- Comparison of N_e profiles for RAM C-III measured at $x/d_N = 4$ with profiles calculated from boundary-layer theory. (Solid symbols show data which, by the criteria, are affected by probe heating.)

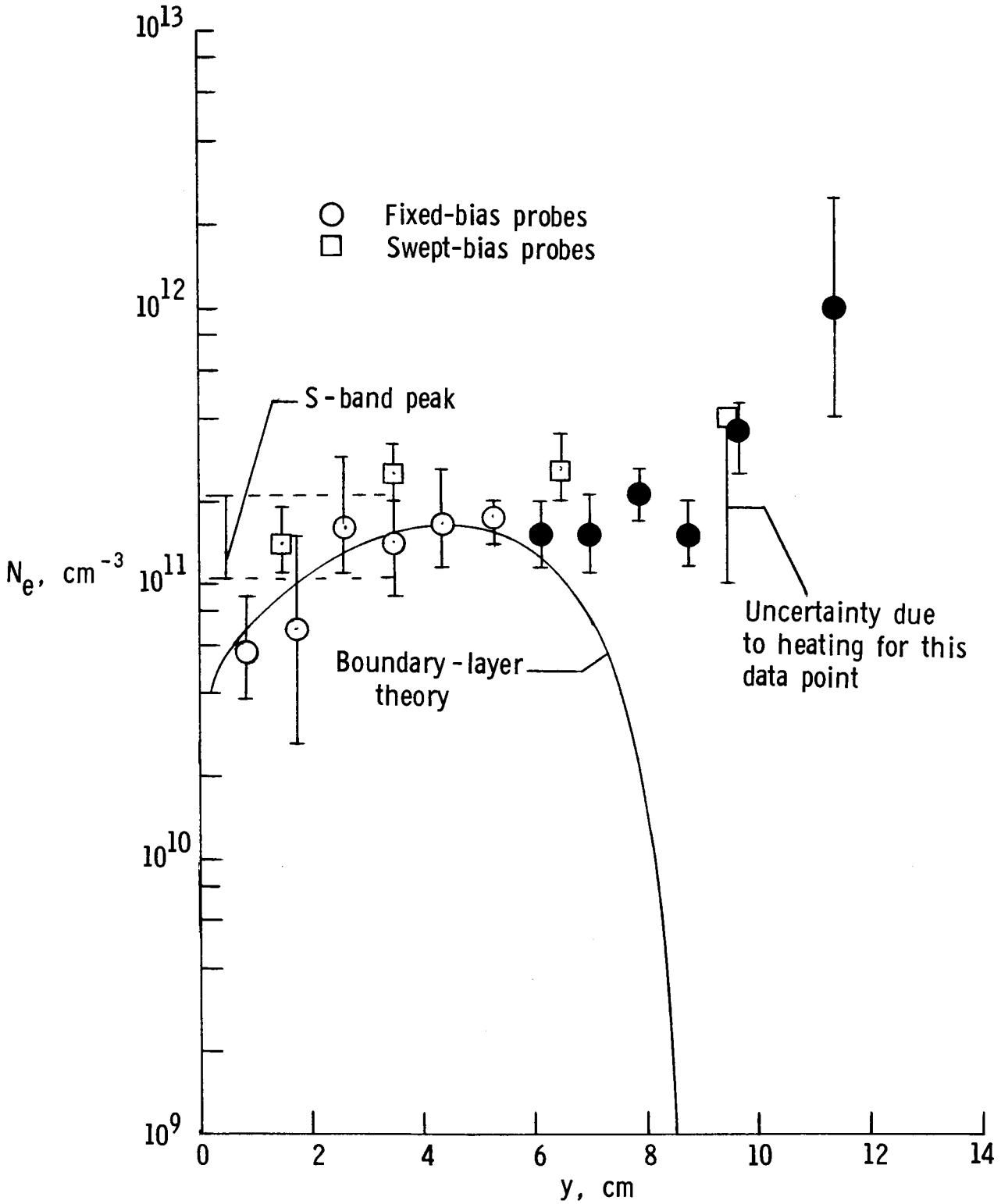

(b) 65.2 km.

Figure 4.- Continued.

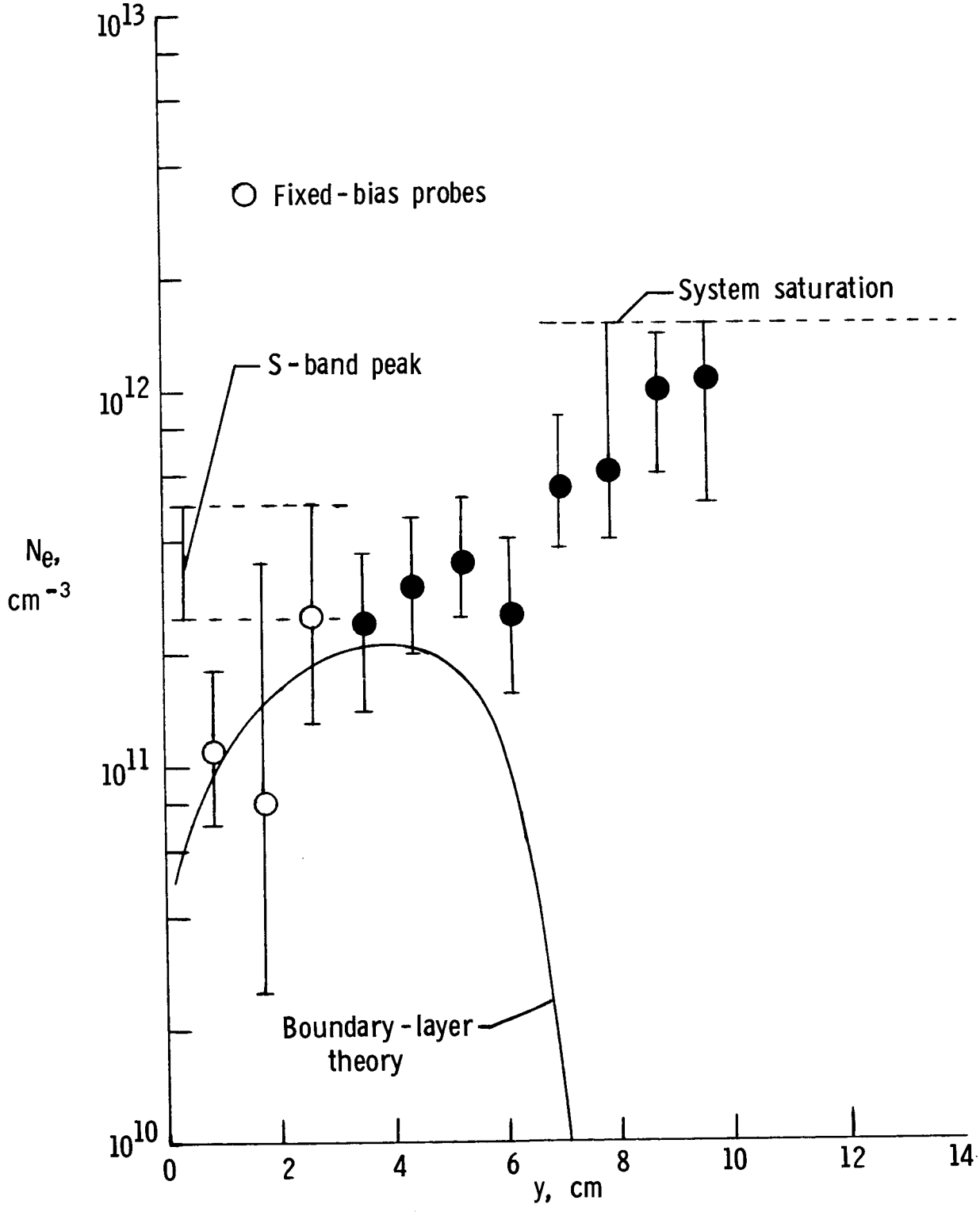

(c) 61.6 km.

Figure 4.- Concluded.

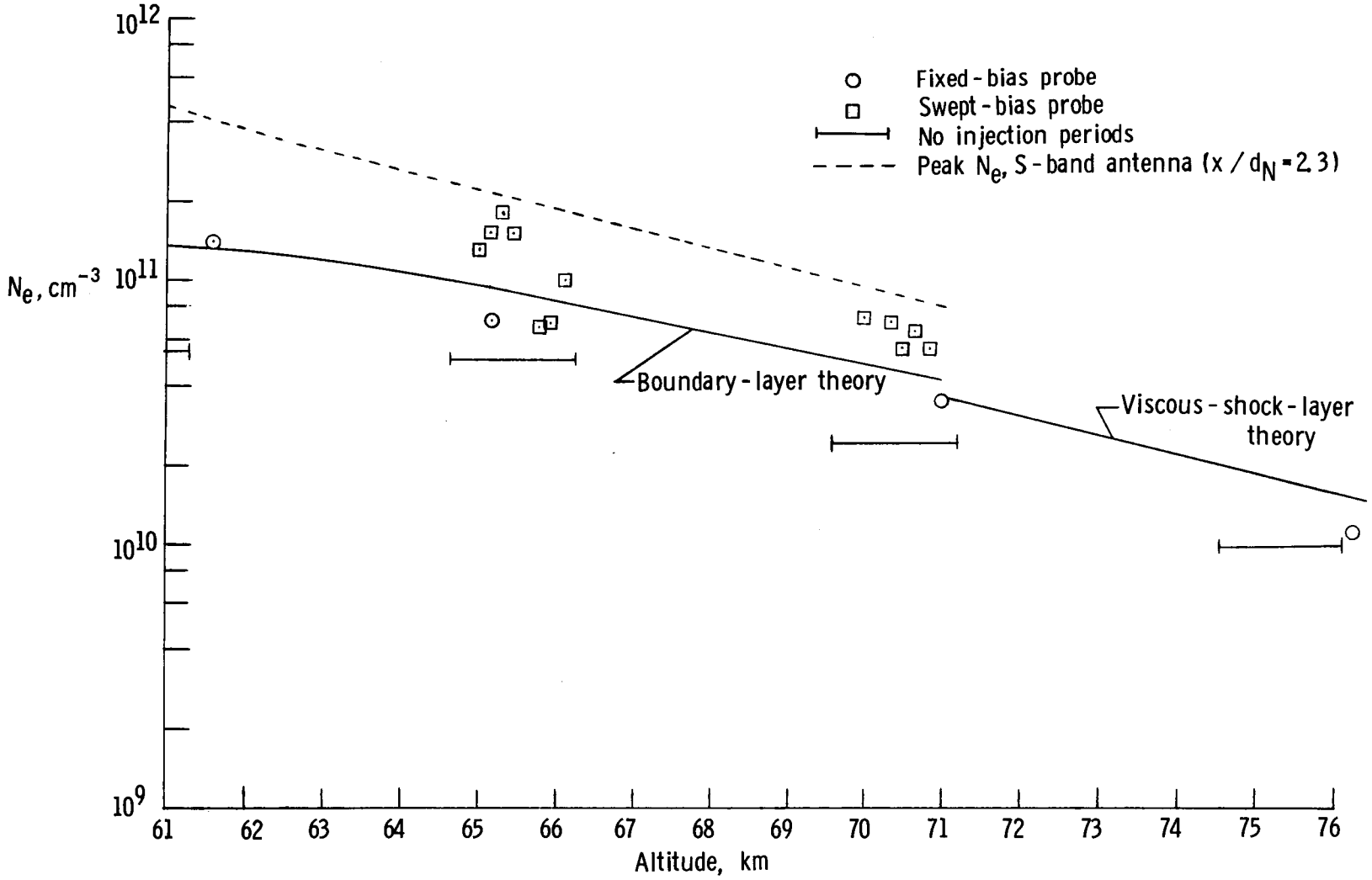

(a) y = 1.5 cm.

Figure 5.- Calculated and measured variation of N_e with altitude at $x/d_N = 4$.

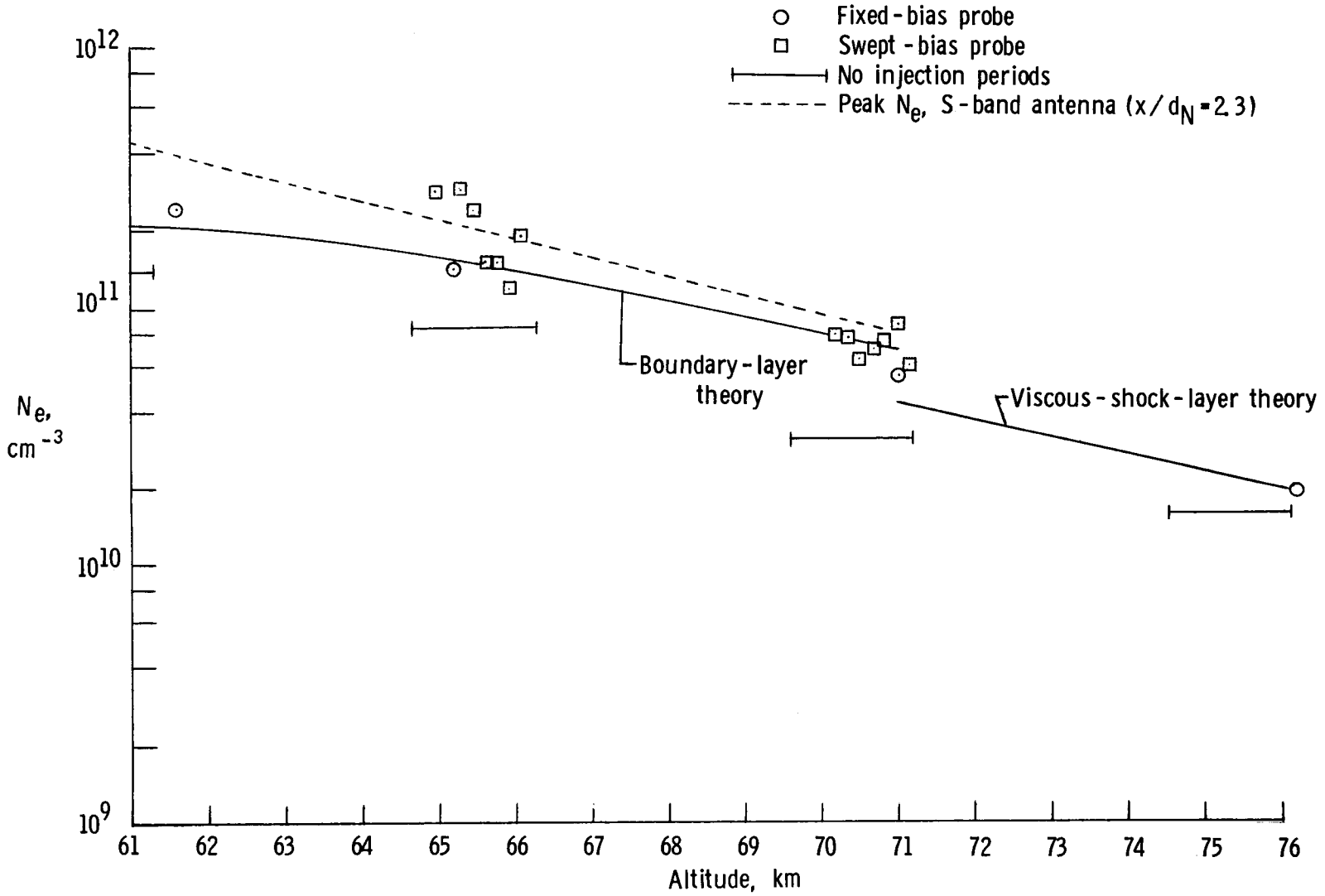

(b) y = 3.5 cm.

Figure 5.- Continued.

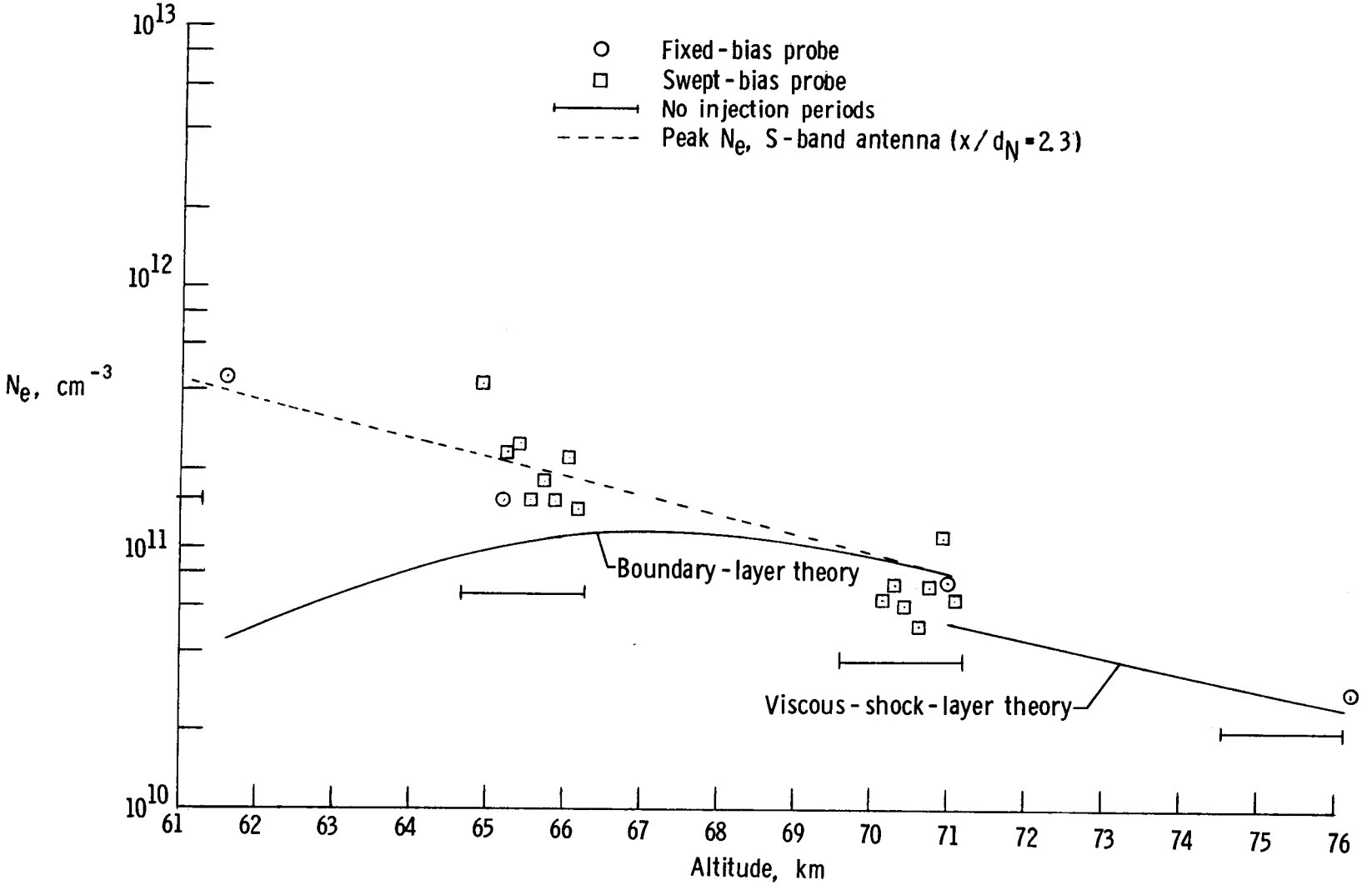

(c) y = 6.5 cm.

Figure 5.- Continued.

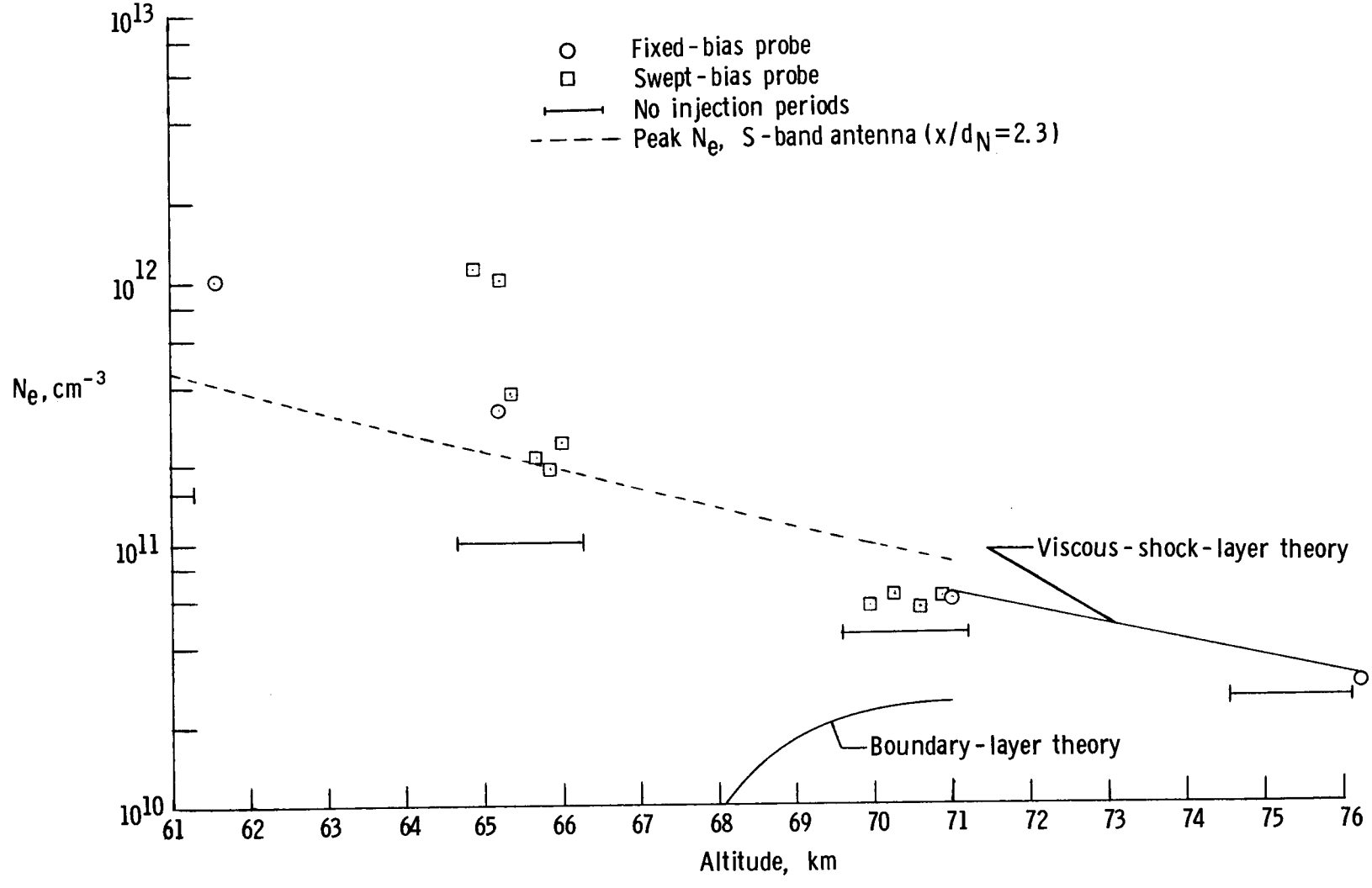

(d) y = 9.5 cm.

Figure 5.- Concluded.

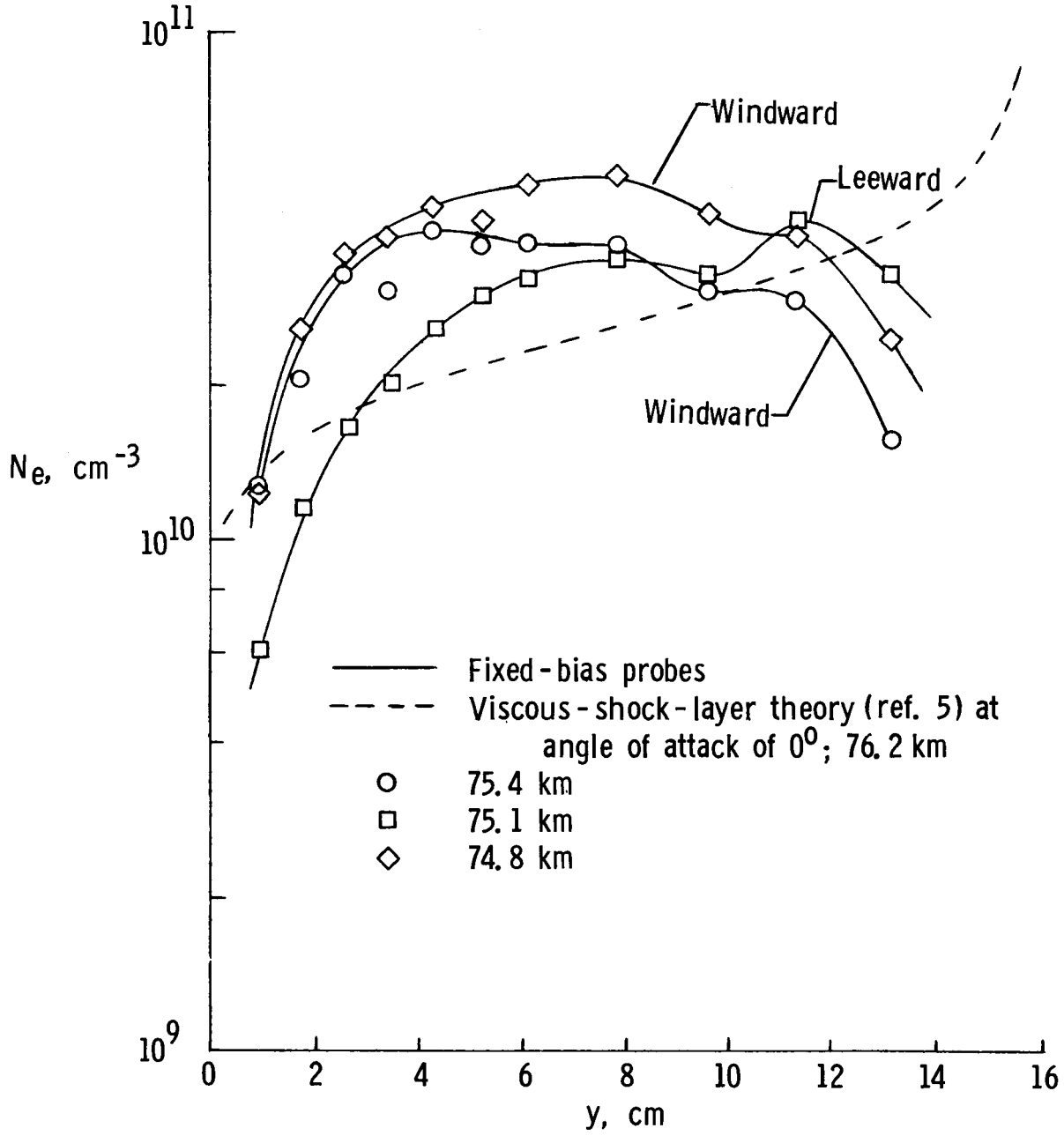

Figure 6.- RAM C-III electron density profiles for different angles of attack.

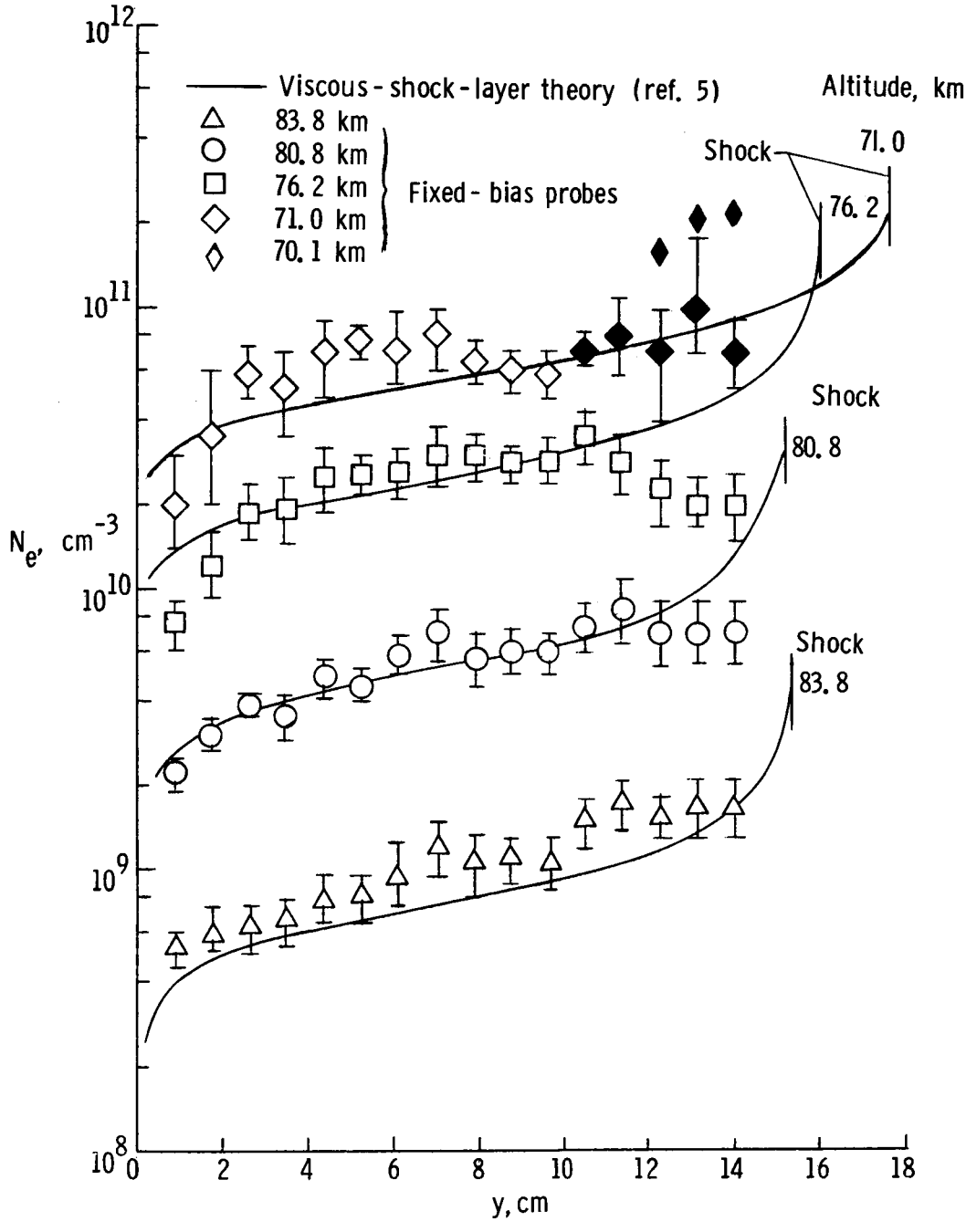

Figure 7.- Profile shape comparison for RAM C-III at $x/d_N = 4$ with fully viscous-shock-layer theory. (Solid symbols show data which, by the criteria, are affected by probe heating.)

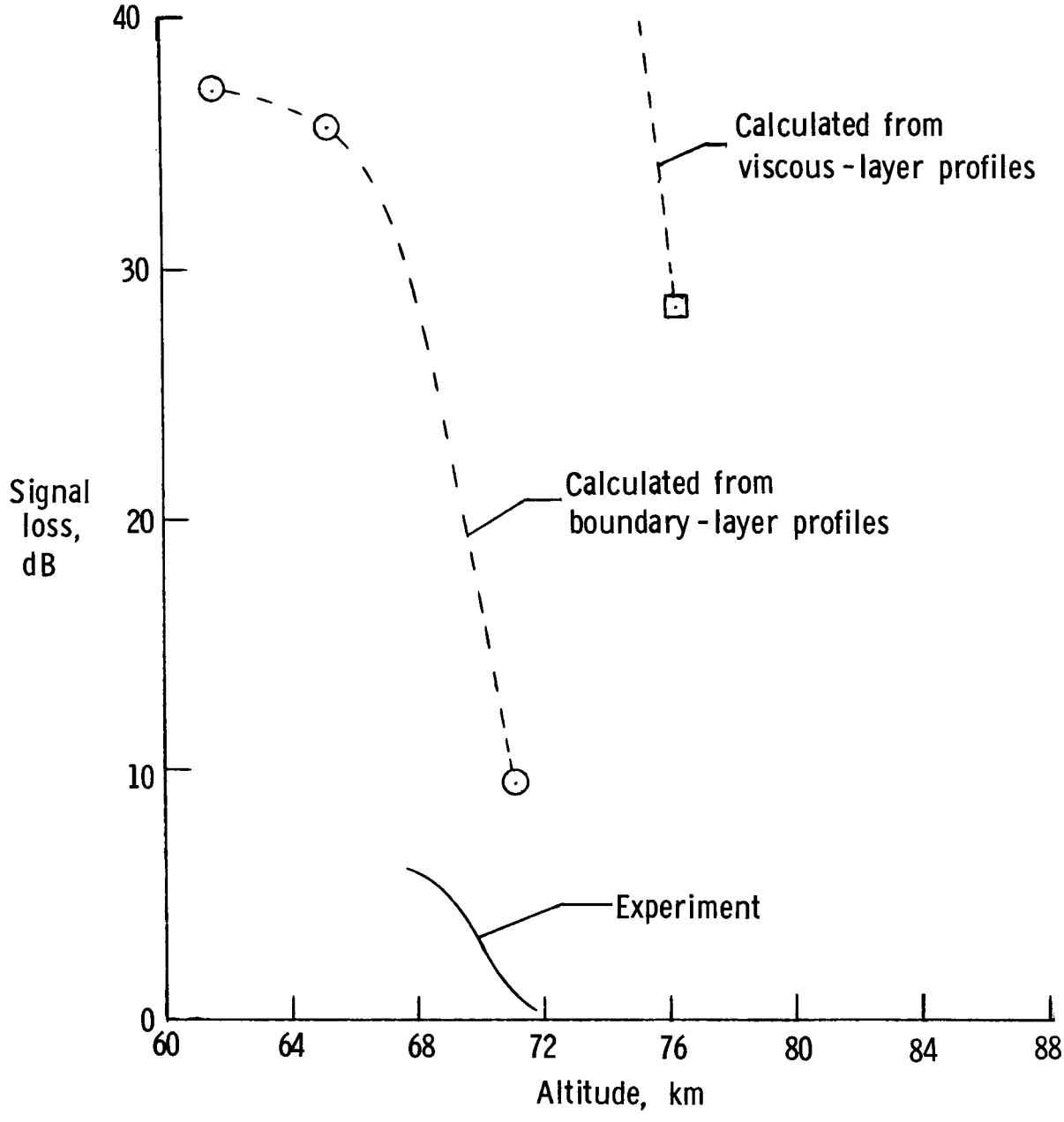

Figure 8.- Experimental and calculated attenuation for S-band antenna at $x/d_N = 2.3$ on RAM C-III.

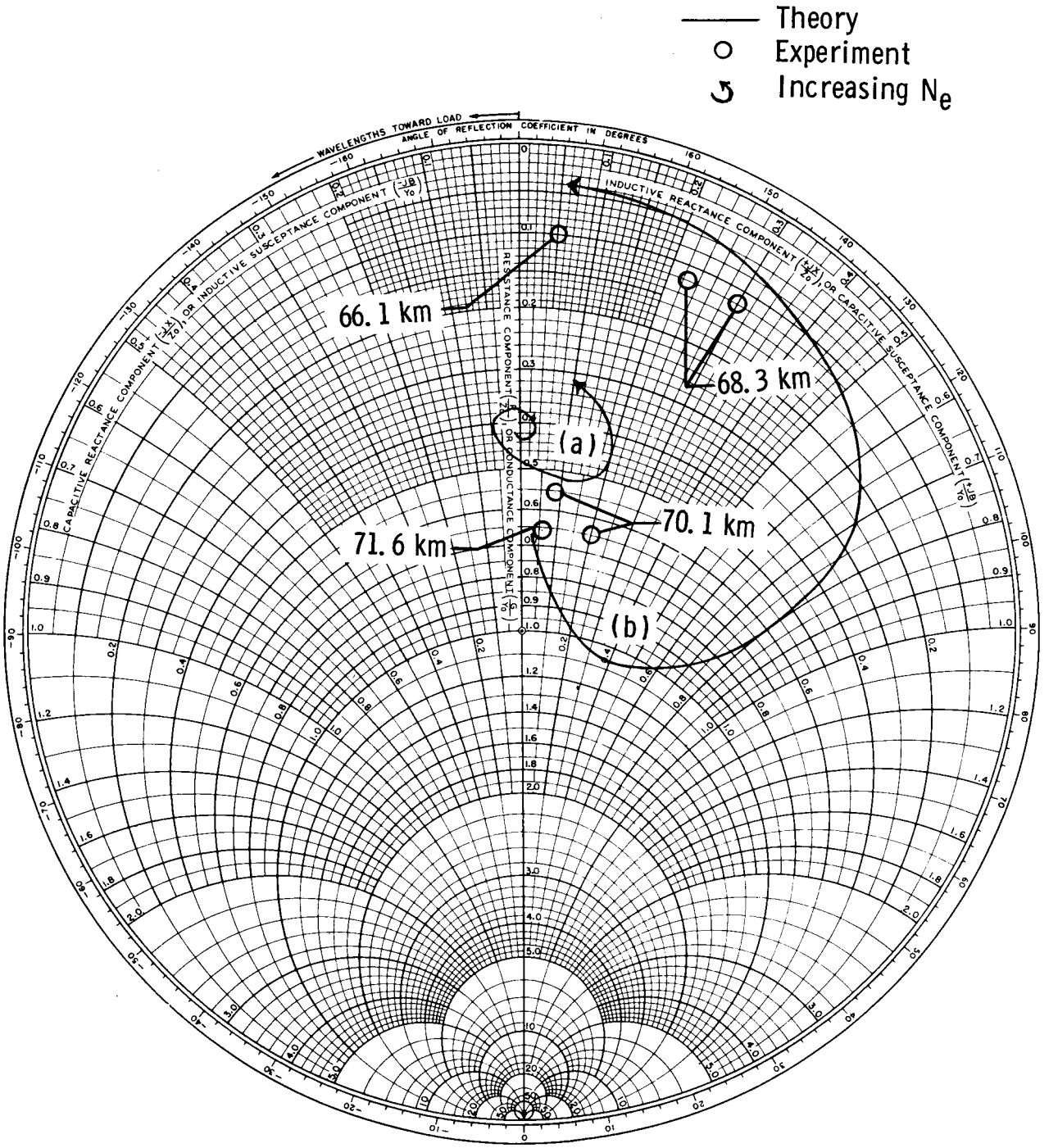

Figure 9.- Variation in admittance of S-band antenna as a function of peak N_e for (a) N_e profiles from reference 5 and (b) N_e profiles from this paper.

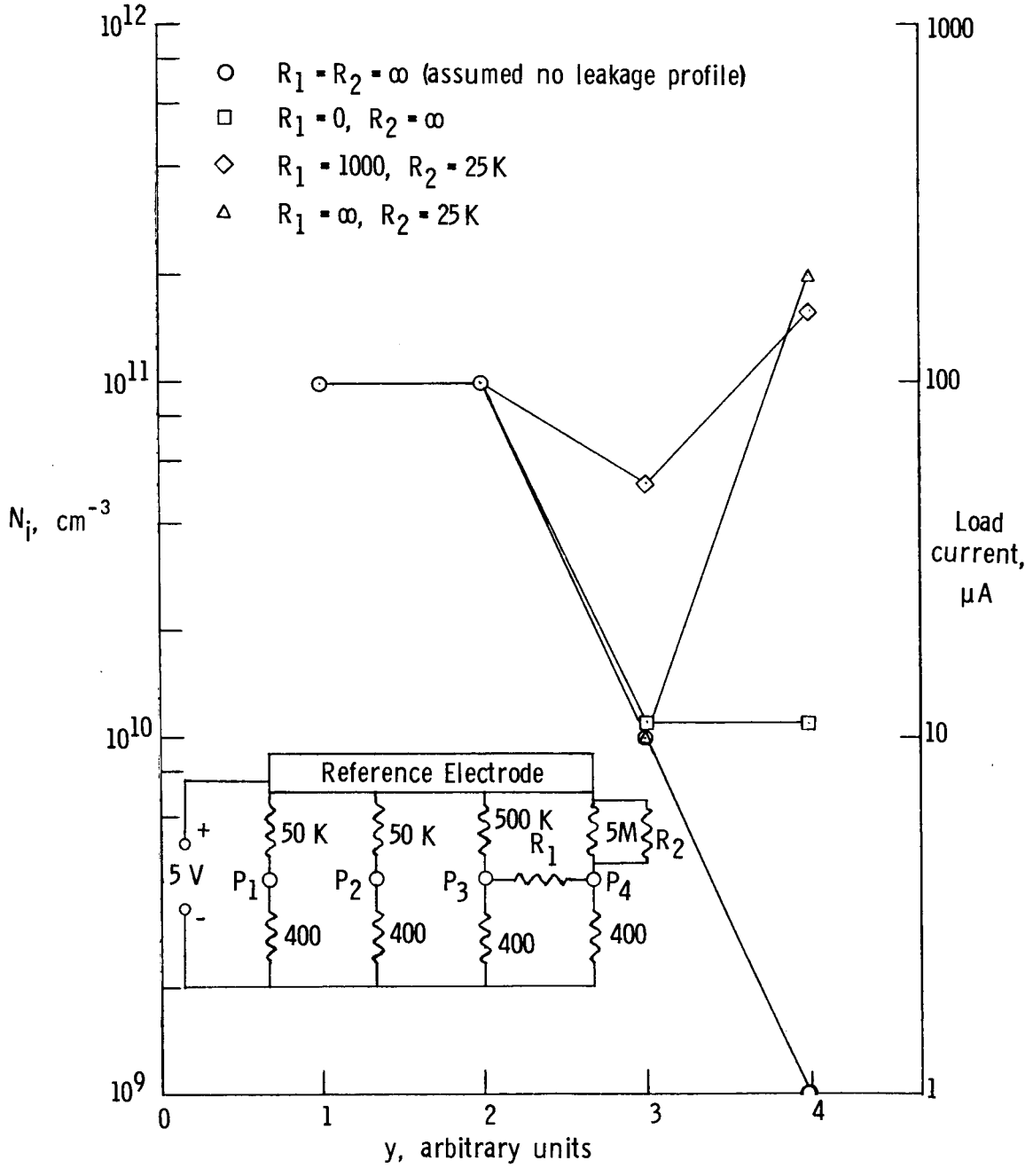

Figure 10.- Effects of surface leakage on outer Langmuir probe profiles for simultaneous bias.

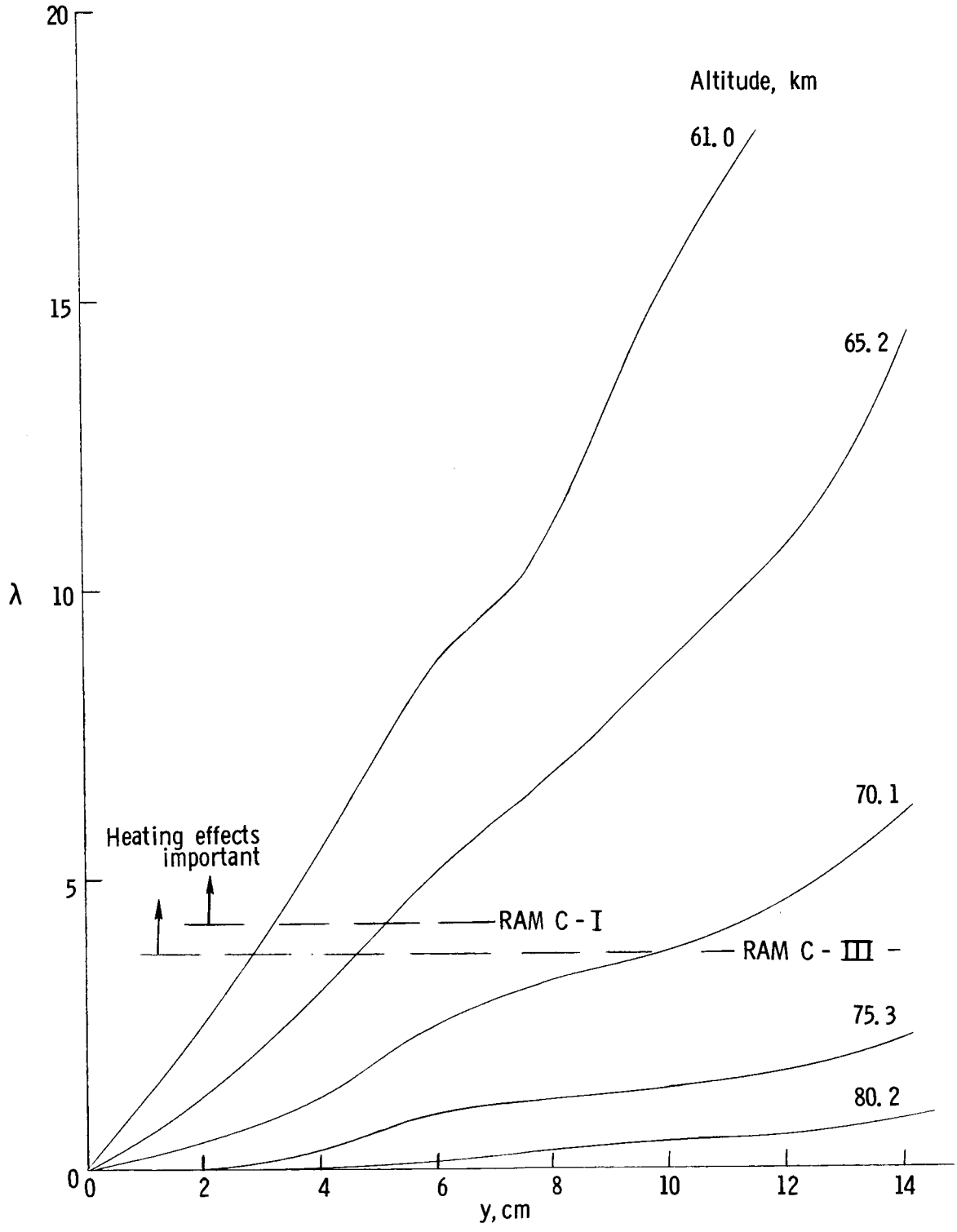

Figure 11.- Calculated relative heat input to probe rakes.

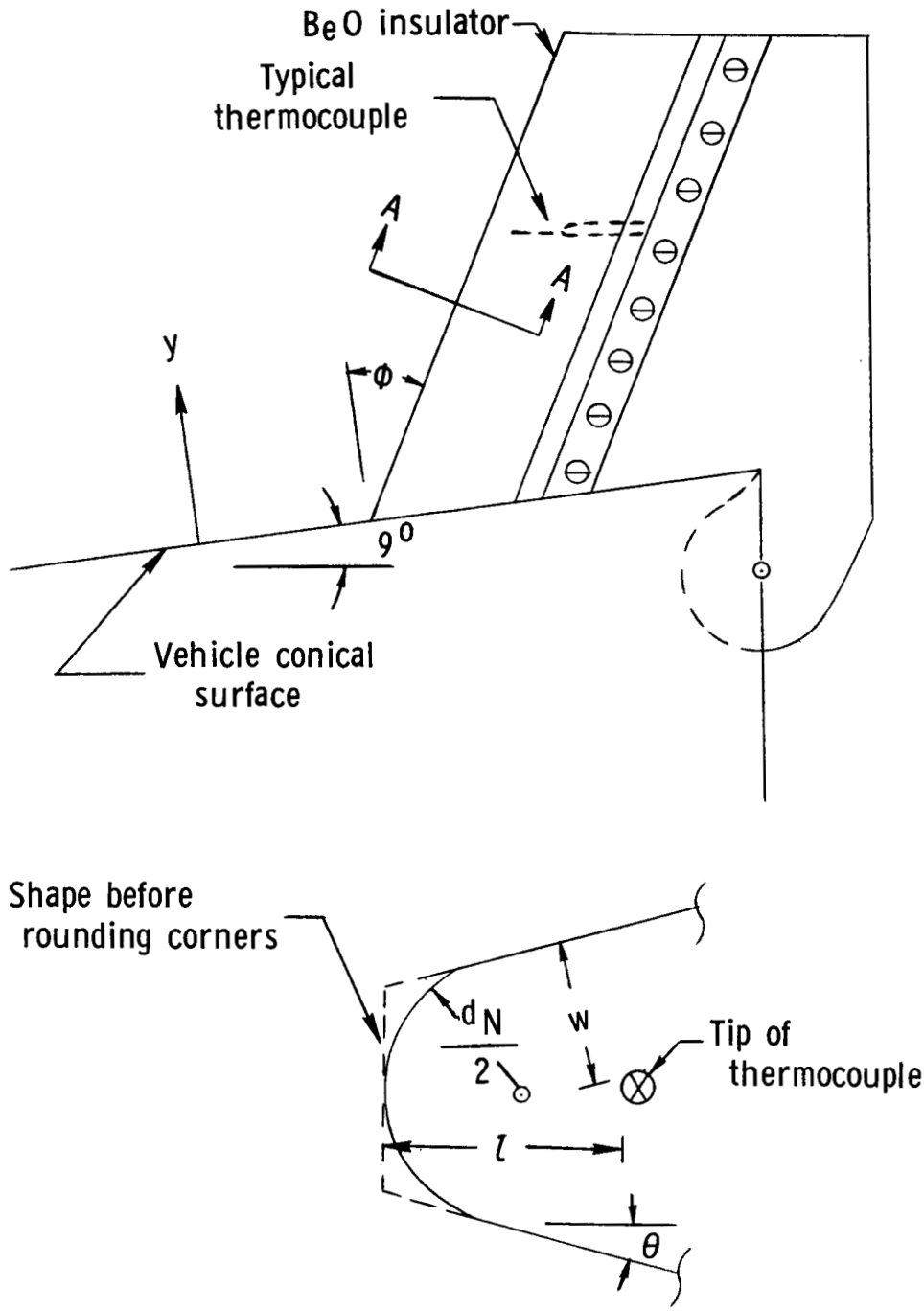

Figure 12.- RAM C thermocouple rakes.

NASA-Langley, 1973 —— 25 L-8792